3-2022

Effects of Long Duration Earthquakes on the Interaction of Inertial and Liquefaction-Induced Kinematic Demands on Pile-Supported Wharves

Milad Souri
GRI

Arash Khosravifar
Portland State University, karash@pdx.edu

Stephen E. Dickenson
New Albion Geotechnical

Nason McCullough
Jacobs Engineering Group

Scott Schlechter
GRI

Citation Details

Published as: Souri, M., Khosravifar, A., Dickenson, S., McCullough, N., & Schlechter, S. (2022). Effects of long duration earthquakes on the interaction of inertial and liquefaction-induced kinematic demands on pile-supported wharves. Soil Dynamics and Earthquake Engineering, 154, 107155.

Effects of Long Duration Earthquakes on the Interaction of Inertial and Liquefaction-Induced Kinematic Demands on Pile-Supported Wharves

Milad Souri[1], Arash Khosravifar[2,*], Stephen Dickenson[3], Nason McCullough[4], Scott Schlechter[5]

[1] Engineering Staff, GRI, Beaverton, OR 97008; e-mail: msouri@gri.com
[2] Corresponding author, Assistant Professor, Department of Civil and Environmental Engineering, Portland State University, Portland, OR 97201; e-mail: karash@pdx.edu
[3] Principal Engineer, New Albion Geotechnical, Inc., Reno, NV 89509; e-mail: sed@newalbiongeotechnical.com
[4] Principal Geotechnical Engineer, Jacobs, Corvallis, OR 97330; e-mail: Nason.McCullough@jacobs.com
[5] Principal, GRI, Beaverton, OR 97008; e-mail: SSchlechter@gri.com

ABSTRACT

Nonlinear dynamic analyses were performed to evaluate the effects of ground motion duration on the dynamic response of a pile-supported wharf subjected to liquefaction-induced lateral ground deformations. The numerical model was first calibrated using recorded data from a well-instrumented centrifuge test, after which incremental dynamic analyses were conducted using a suite of spectrally matched motions with different durations. The nonlinear dynamic analyses were performed to evaluated three loading scenarios: combined effects of inertial loads from the wharf deck and kinematic loads from ground deformations, deck inertial loads only in the absence of liquefaction (with minimal kinematic loads), and kinematic loads only in the absence of deck mass inertia. The analysis results were evaluated to provide insights on the relative contribution of inertial and kinematic demands on the response of the wharf with respect to motion duration. It was found that the contribution of peak inertial and peak kinematic loads to the maximum total demand increases only slightly with motion duration and intensity. The response of the wharf was

* Corresponding author.
E-mail address: karash@pdx.edu (A. Khosravifar)

found to be primarily governed by kinematic demands when subjected to long-duration motions for the type of foundation analyzed in this study which is commonly used in the port industry.

Keywords: Liquefaction, pile-supported wharf, inertia and kinematics interaction, long-duration ground motions

1.0 INTRODUCTION

The damage to pile-supported bridges and wharves due to liquefaction-induced lateral spreading has been documented in a number of case histories, e.g., 1989 Loma Prieta earthquake (Donahue et al. 2005), 1995 Kobe earthquake (Tokimatsu and Asaka 1998), 2010 El Mayor-Cucapah earthquake (Turner et al. 2016), 2014 Chile earthquake (Morales et al. 2020), and 2016 Kaikoura earthquake (Cubrinovski et al. 2017). In most of these studies, the lateral spreading displacements exceeding 1 m was reported as the likely cause of damage. In some case histories, the acceptable performance of piles was attributed to design for either earthquake shaking (inertia) or post-liquefaction lateral spreading (kinematic), as shown by Finn (2005) for undamaged bridge piles in the 1983 Nihon-Kai-Chubu earthquake. This study focuses on the combination of inertial and liquefaction-induced kinematic demands. Below is a summary of studies that have focused on the interaction of these two loads on pile foundations.

MCEER/ATC (2003) states that, for most earthquakes, the peak inertia is likely to occur early in the ground motion, while the maximum lateral spreading load will develop near the end of motion. It recommended designing piles for independent effects of inertia and lateral spreading. However, it acknowledged that the two loads may interact during long-duration shaking events.

A series of 14 centrifuge tests on piles in liquefiable soils was performed at UC Davis by Boulanger and coworkers from 1997 to 2006. Using the results of these tests, Boulanger et al. (2007) and

Ashford et al. (2011) recommended combining the lateral spreading load with a fraction of inertia in contrast to the recommendations put forth in MCEER/ATC (2003).

Researchers at Rensselaer Polytechnic Institute (RPI) performed many centrifuge tests on piles in liquefiable soils. In one series of tests, Abdoun and Dobry (2002) showed that while the bending moments at depths shallower than 2 or 3 m are affected by superstructure inertia, this effect disappeared for bending moments at deeper depths for 0.6-m-diameter piles. They also reported a post-peak reduction in the lateral spreading force despite the increase in ground displacement (Dobry et al. 2003; Abdoun et al. 2003). Olson et al. (2017) performed another series of four centrifuge tests at RPI to investigate the magnitude of lateral spreading force on large-diameter foundations and proposed revised method to estimate limiting lateral pressures. The latter tests focused on the kinematic effects, and the effects of inertia were not considered.

Tokimatsu and coworkers performed large-scale 1-g shake table tests in Japan's NIED facility to study phasing of inertia and liquefaction-induced lateral spreading (Tokimatsu et al. 2005). They concluded that the ground displacement tends to be in-phase with the superstructure inertia (increasing the stresses in piles) when the natural period of the structure (T_b) is shorter than the natural period of the ground (T_g), and the ground displacements tend to be out-of-phase with the superstructure inertia (restraining the pile stresses from increasing) when T_b is larger than T_g.

Vytiniotis et al. (2019) evaluated a mitigation strategy for damage to typical pile-supported wharves subjected to lateral spreading and structural response. They used an uncoupled numerical approach where the free-field and structure responses were analyzed separately. They concluded that using an uncoupled approach provides significant computational advantages over the full three-dimensional (3D) analysis for simulating soil-structure interaction. Shafieezadeh et al. (2012) performed a similar uncoupled two-dimensional (2D) simulation to evaluate the seismic performance of pile-supported wharf structures. They concluded that the liquefaction-induced lateral ground deformation was an important source of damage to the piles. They indicated that the pile-deck connection and the pile sections near the interface between loose and dense sand layers are susceptible to severe damage. In our study, a coupled analysis approach is used since the interaction of inertial and kinematic demands during motion is the important mechanism that is investigated in this paper.

Despite significant achievements made to investigate the interaction of inertial and liquefaction-induced kinematic loads on piles, there is currently no consensus in seismic design guidelines on how to combine the two loads in design. This is due in part to the site-, ground motion-, and project-specific nature of the interaction between inertial and kinematic demands as evidenced in varying recommendations provided by maritime and highway transportation agencies. For ports, ASCE COPRI 61 (2014) acknowledges the likelihood of the combination of the two loads and recommends evaluating this assumption on a project-specific basis. For bridge foundations, AASHTO (2014) recommends designing piles for the simultaneous effects of inertia and lateral spreading only for large-magnitude earthquakes (M>8). Washington DOT (WSDOT 2021) acknowledges that the two loads are more likely to interact during long-duration motions; using earthquake magnitude as a proxy for duration, it recommends combining 100% kinematic with 25% inertia when earthquakes with M>7.5 contribute to more than 20% of the hazard for peak ground acceleration. Caltrans recommended 100% kinematic + 50% inertia (Caltrans 2012), but this recommendation was retracted in favor of higher performance criteria (Caltrans 2016).

The effect of motion duration on the interaction of inertial and kinematic loads is particularly important in highly seismic regions like the Pacific Northwest of the United States, where the probabilistic seismic hazard includes significant contributions from the Cascadia Subduction Zone, which is expected to produce a long-duration Magnitude 9 earthquake. Khosravifar et al. (2014) and Nasr and Khosravifar (2017) studied the effects of ground motion duration on inelastic pile demands on relatively stiff large diameter shafts in liquefied soils and found that inelastic pile demands are amplified in long-duration earthquakes due to incremental yielding in the plastic hinge. Dickenson et al. (2014) examined the effects of long-duration motions on the seismic performance of a wharf structure at the Port of Los Angeles in a testbed study and found that plastic hinges in piles (0.6 m concrete piles) formed generally once the ground displacements passed a threshold of approximately 0.3 m. They found that for earthquake motions with an average 475-year return period (contingency level earthquake (CLE) motions for a “High” hazard classification per ASCE61-14), this threshold occurred after approximately 4 to 10 seconds of significant shaking and Arias Intensity of 0.9 to 1.2 m/sec.

The primary objective of this study is to extend the breadth of the previous studies to investigate the effects of inertial and kinematic load interaction on pile-supported wharves subjected to short- and long-duration earthquake motions. First, a numerical model was developed and calibrated against a centrifuge test on a pile-supported wharf subjected to short-duration earthquake shaking. Then, numerical analyses were performed using a suite of spectrally matched ground motions covering a wide range of strong motion durations. The nonlinear dynamic analyses were performed for three loading cases: (a) a case with combined effects of liquefaction-induced lateral spreading and wharf deck inertia, (b) a case with wharf deck inertia only in the absence of liquefaction, and (c) a case with liquefaction but without wharf deck inertia. It is important to note that even in nonliquefied conditions, the piles are subjected to kinematic demands from the dynamic response of the soil profile as shown by a vast body of literature, such as Makris and Gazetas (1992), Wang et al. (1998), and Bentley and El Naggar (2000). In this paper, the term “kinematic” is used to define the demands on piles due to liquefaction-induced lateral ground deformations (i.e., Displacement Demand), and the term “inertia” is reserved to define the inertial loads associated with the deck mass. Incremental dynamic analyses were performed by linearly scaling the spectrally-matched motions to three different levels of shaking to evaluate the effect of timing of liquefaction triggering. The main contribution of this study is the quantification of the effects of ground motion duration and intensity on the contribution of lateral spreading and inertial loads on pile demands for a typical pile-supported wharf structure. Considering the soil- and structure-specific nature of the interaction of inertial and kinematic loads, this study provides a benchmark, validated with centrifuge experiments, that can be used by Port engineers in project specific applications.

2.0 DEVELOPMENT OF NUMERICAL MODEL

A 2D numerical model was developed using Fast Lagrangian Analysis of Continua (*FLAC)* numerical analysis software (Itasca, 2016) and was calibrated using a centrifuge test of a pile-supported wharf structure subjected to a short-duration ground motion (Test NJM01 in McCullough et al. 2000). The numerical modeling presented in this calibration study is considered Class-C1 prediction based on Lambe (1973) since centrifuge test results were available during model development.

2.1 Overview of the Centrifuge Test

The centrifuge model configuration in this test is shown in Fig. 1. It consisted of a multi-lift rock dike, a dry dense sand layer (relative density, D_R = 82%), overlying a liquefiable loose sand layer (D_R = 39%), overlying a dense sand layer (D_R = 82%). A set of 21 piles in a 7-by-3 configuration support the wharf deck. The piles were made with aluminum pipes having an outer diameter (D) of 0.64 m, a wall thickness (t) of 0.036 m, and a length (L) of 27.2 m (in prototype scale). The piles were equally spaced at approximately 10 diameters (10*D*; equivalent to 6.1 m) center-to-center in the direction parallel to the slope and 8 diameters (8*D*; equivalent to 5.1 m) in the direction perpendicular to the slope as shown in the plan view. The model was subjected to a series of spin up and spin down events with low-amplitude sinusoidal excitations in between to check the data acquisition system. The model was then spun up to a centrifugal acceleration of 40.1 g and was subjected to a sequence of earthquake shaking with increasing amplitudes. The first shaking event (Event 11) with a base acceleration of 0.138 g in prototype scale was modeled in this study. The inferred failure surface, interpreted from the peak transient soil displacements obtained from accelerometer arrays, is shown with a dashed red line in Fig. 1 which illustrates how liquefaction-induced kinematic demands are applied to the piles. The accelerations, displacements, and stresses reported in this study are in prototype scale which are converted following scaling laws described in Kutter (1992). Details about this centrifuge test can be found in McCullough et al. (2007) and the data report in McCullough et al. (2000). Data from this centrifuge tests was thoroughly re-evaluated and vetted in the current study prior to the calibration, using current procedures for the analysis and interpretation of centrifuge modeling. The key characteristics of soil, pile, wharf deck and input motion are listed in Table 1.

2.2 Overview of Numerical Model Calibration

A two-dimensional (2D), plane-strain, fully coupled, effective-stress, dynamic model was created in *FLAC* to model the centrifuge experiment described above. In the model geometry and discretization of the soil mesh shown in Fig. 2, the soil and container of the centrifuge test were modeled by 2D continuum elements, and the piles and deck were modeled using beam elements. The pile nodes were connected to the soil mesh using soil interface non-linear springs.

2.2.1 Soil Constitutive Model

The pressure-dependent multi-yield surface model (PDMY03) was used to model the cyclic shear behavior of sands and rockfill with different relative densities during the earthquake motion. The original constitutive model was developed and calibrated against a dataset of laboratory and centrifuge tests by Elgamal et al. (2003) and was updated by Khosravifar et al. (2018). The yield criterion in the employed soil model is based on the multi-surface plasticity framework. The model incorporates a non-associative flow rule in order to simulate the mechanism for the post-liquefaction accumulation of shear strains and the subsequent dilation in liquefied soils. The primary focus in the calibration of the soil model was to capture the triggering of liquefaction and post-liquefaction accumulation of shear strain. The loose sand was calibrated to trigger liquefaction (defined here as 3% single amplitude shear strain) in 15 cycles at a cyclic resistance ratio (CRR; defined as the cyclic shear stress to trigger liquefaction normalized by the initial vertical effective stress) of 0.10 estimated from the correlations by Idriss and Boulanger (2008). Fig. 3 provides an example result of a single-element undrained cyclic direct simple shear (CDSS) simulation for sand with D_R = 39% (corresponding to energy- and overburden stress-normalized standard penetration test blow count of $(N_1)_{60}$=7) under a vertical effective stress of 100 kPa. Fig. 3a shows the cyclic stress ratio (CSR) versus the number of uniform loading cycles, which was calibrated to trigger liquefaction at the desired CSR in 15 cycles. The stress–strain loops and the stress path responses are shown in Fig. 3b and 3c, respectively. The results for cyclic stress ratio versus shear strain shown in these figures indicate that the model produces post-liquefaction plastic shear strain accumulation of approximately 1% to 1.5% per cycle after liquefaction is triggered. It will be shown later that the calibrated model reasonably estimates the permanent liquefaction-induced soil displacements in the centrifuge test. The shear moduli of the soil units were defined based on the Seed and Idriss (1970) relationship, using the soil modulus coefficient (K_{2max}) values reported in Table 2. The shear wave velocity (Vs) profile calculated using these shear moduli generally agreed with the Vs measurements from the centrifuge test. The soil model input parameters are summarized in Table 2. More details for each input parameter can be found in Khosravifar et al. (2018).

2.2.2 Wharf Deck and Pile Elements

The wharf deck was modeled with elastic beam elements using the properties listed in Table 1. The piles exhibited elastic behavior in the centrifuge test and were modeled as elastic in the numerical model that was used for validation (the piles were modeled as elasto-plastic in the subsequent incremental dynamic analysis as described later). The piles were modeled using beam elements in *FLAC* connected to soil mesh using interface springs. Based on the rigidity of the wharf deck and pile to deck connection, the pile head connections to the wharf deck were modeled as fixed head condition. The pile tips were fixed in the vertical direction given that the pile tips were at the container base, however they were free to rotate.

In the 2D *FLAC* model, it was assumed that the mass of the deck was equally distributed between the three rows of piles. To implement this assumption, the deck was defined with 1/3 of the actual total mass, and the "spacing" parameter for pile elements in *FLAC* was set to 6.1 m which is the center-to-center spacing between the piles in the out-of-plane direction (note that this modeling approach in *FLAC* is equivalent to setting the out-of-plane thickness of the soil mesh to 6.1 m).

2.2.3 Soil Interface Elements

Modeling in 2D has the advantage of being computationally more efficient than modeling in 3D and it simplifies the interpretation of results. However, to account for large deformations of the soil mesh and the ability of the soil to "flow" around the piles, nonlinear soil springs were used to capture the lateral interaction between the piles and soil, and to approximate the 3D effects of soil deformation around the piles. The p-y spring properties were based on American Petroleum Institute (API 1993) recommendations for sand; however, the moduli of the subgrade reaction were modified from API to account for the difference in behavior between the local soil interface and the rest of the soil mesh. The final spring parameters were based on calibration to four pseudo-static lateral load tests that were performed in two centrifuge tests by McCullough et al. (2001) with very similar soil and pile properties to the centrifuge test used in this study. The modulus of subgrade reaction was selected to be 3900 kN/m^3 for the loose and dense sand and 5800 kN/m^3 for rockfill. More details on the back-calculation of the moduli of subgrade reaction from the centrifuge tests are provided in Souri et al. (2020). The p-y strengths (i.e. P_{ult}) were developed based on the friction angles reported in Table 2. A pseudo-cohesion of 15 kPa was incorporated as a practical, yet adequate, approximation for calculating the ultimate soil reaction in rockfill to account for additional resistance caused by the interlocking and movement of rock particles near the ground surface (McCullough and Dickenson 2004). Slope effects on the stiffness of p-y springs were accounted for as described in McCullough and Dickenson (2004). No additional multipliers were applied in the liquefiable soils, as the first-order softening effects of liquefaction were assumed to be captured by the soil elements connected to the free end of the p-y springs. The advantage of using this modeling approach compared to assigning a constant p-multiplier to p-y springs is that the time-dependent softening of soil elements due to the generation of excess pore water pressure during the earthquake time history is better captured. The backbone curve for the soil interface elements in *FLAC* (i.e., p-y springs) is characterized using a bi-linear relationship with the same stiffness used for the loading and unloading behaviors. The soil interface elements in *FLAC* have the capability of modeling the gap formation during cyclic loading such that a gap that is formed on one side of the pile during lateral spreading needs to close before lateral soil reactions can develop upon load reversals.

The piles in the centrifuge model were in contact with the base of the centrifuge box which is representative of end-bearing piles tipped in a competent rock layer in field conditions. Therefore, the pile tips in the baseline numerical model were simply fixed in the vertical direction without any side shear and end bearing soil springs. A sensitivity analysis was performed by removing the pile tip fixity in the vertical direction and adding vertical side shear and end bearing springs which showed minimal differences in the natural period of the wharf deck and the peak wharf acceleration, likely because the lateral behavior of the wharf system is dominated by the flexural response of the piles. This modeling approach resulted in a reasonable agreement between the numerical model and the centrifuge test results, as will be explained in a later section.

2.2.4 Modeling Centrifuge Container

The approach presented by Boulanger et al. (2018) was followed to calculate the equivalent 2D properties of the centrifuge container. The centrifuge model employed a flexible shear beam container, which consisted of six rigid aluminum rings separated by a 12-mm (model scale) soft layer of 20-durometer neoprene rubber. The container included vertical shear rods to facilitate transfer of vertical shear forces to the soil. The container nodes with the same elevation on the left and right sides of the model were attached to have identical vertical and horizontal movements. The aluminum ring and rubber rings were modeled as linear elastic materials. It was important to model the interface between the soil elements and the container elements in a way that allows for slippage and simulates an impermeable boundary between the soil and the container. To do so, extremely flexible beam elements were placed between the soil elements and the container elements in the *FLAC* model. One side of each beam element was attached to a soil element using a frictional interface element with a friction angle of 23 degrees, which was approximately two-thirds of the friction angle in the soil elements. The other side of each beam element was glued to a container element. This modeling approach allowed for relative displacement between soil and beam elements and restricted the relative movement between the beam and container, and it provided an impermeable boundary at the interface. The beam element properties were selected to be extremely flexible such that they would have no effect on the container response.

2.2.5 Damping

A relatively small mass and stiffness proportional Rayleigh damping (0.5%) was employed in soil elements at a center frequency of 1.25 Hz corresponding to the natural period of the wharf system. While the natural period of the system changes before and after triggering of liquefaction, the assigned damping (equivalent to 1% damping at 0.3 Hz and 5 Hz) applies a small amount of damping over the periods of interest to account for small-strain damping and reduce numerical noise. A nominal 2% damping was applied to the structural elements using a mass proportional Rayleigh damping at a center frequency of 1.25 Hz. Past studies have shown the importance of accounting for the radiation damping to represent the loss of energy due to outgoing waves transmitted from the pile to the soil medium (e.g., Gazetas and Dobry 1984; El Naggar and Novak 1996; Wang et al. 1998). The radiation damping can be modeled using dashpots distributed over the length of the piles as explained by Boulanger et al. (1999) where the dashpot coefficients can be assigned based on the recommendations of Gazetas and Dobry (1984). While some numerical platforms have the capability of modeling this damping using distributed dashpots along the piles (e.g., Brandenberg at el. 2013; Shafieezadeh et al. 2012), this damping was approximated in the 2D analysis in *FLAC* using an additional mass proportional Rayleigh damping. First, the viscous radiation dashpot coefficients were calculated along the pile using depth varying values equal to $4\rho DV_s$ with Vs taken as 10% of the pre-earthquake values to account for the softening effects of pore water pressure generation in the soil units. Next, the damping ratio of the first mode of vibration was calculated as 13% using $\zeta = C/(2Mw)$ where C and M are the modal damping and mass matrices calculated for the first model of vibration and w is the natural angular frequency (Chopra 1995). The nominal 2% structural damping and 13% radiation damping were only applied to the structural elements (i.e. piles and deck). Sensitivity analysis confirmed that using these damping ratios provided a reasonable match between wharf accelerations computed from simulations and recorded in centrifuge test. The large amount of deformation experienced in liquefied soil and laterally spreading rockfill further justifies the use of this damping.

2.3 Comparison of Numerical and Experimental Results

The main objective in calibration of the numerical model was to ensure that key responses important to study the interaction of inertial and liquefaction-induced kinematic demands are reasonably captured. These key responses include amplitude and timing of peak accelerations and peak displacements at the wharf deck and soil surface, and triggering of liquefaction in the loose sand. Therefore, the calibration of the numerical model presented in this section is only focused on the comparison of the mentioned responses between the numerical model and the centrifuge test.

Fig. 4 presents a comparison of the time histories of selected dynamic responses computed from *FLAC* against those measured in the centrifuge test. The figure illustrates (from bottom to top) horizontal acceleration at the base, excess pore pressure ratio (r_u) in the middle of the loose sand layer, horizontal acceleration and displacement at the wharf deck, and horizontal acceleration and displacement at or near the ground surface. All reported displacements are relative to the base of the model. The location of the sensor where the centrifuge data was recorded is shown using a diagram inside each plot.

It can be noticed from this figure that the computed soil and wharf displacements slightly under-predict the peak (transient) recorded soil and wharf displacements in the bayward direction (negative displacements); however, the computed permanent displacements for both soil and wharf deck are in close agreement with the recorded data from centrifuge test. The pattern of computed displacements with time reasonably predicts the recorded displacements from the centrifuge test, including the timing of the critical cycle(s) and the apparent natural period of the soil profile and the pile–wharf system. The simulation results do not predict the strong transient response in the centrifuge recordings, exhibited by large cycles in the upslope direction. Our sensitivity analysis showed that the transient behavior can be improved by softening the lower dense sand (i.e., modeling it with a lower shear modulus); however, we decided to keep the baseline numerical model based on a shear modulus corresponding to a relative density of D_R = 82%, which was calculated during the construction of the centrifuge model.

A comparison of the measured and computed horizontal acceleration time histories at a location near the surface indicates that the main cycles and period are captured reasonably well. However, the simulations have stronger high-frequency components, which resulted in over-predicting the magnitude of peak ground acceleration (PGA) by a factor of 1.2. This high frequency component appears close to the ground surface and is likely attributed to the dynamic response of the top rings of the centrifuge container in the *FLAC* simulations (results of sensitivity analysis with free-field conditions, excluding the container did not exhibit this high frequency). The simulated and measured horizontal accelerations at the wharf deck are in close agreement in terms of both amplitude and frequency.

It can also be noticed from this figure that the pore pressure ratio computed by *FLAC* reasonably matched the recorded pore pressure ratio in the centrifuge test. The difference between the computed and recorded maximum pore water pressure ratios is attributed to the drainage of the excess pore water pressure into the rockfill, which has a higher permeability, during shaking as indicated by the decline in pore pressure ratio towards the end of motion in the centrifuge test. It is worth noting that drainage (flow) was not permitted during the dynamic simulations in *FLAC*.

3.0 DEVELOPMENT OF NUMERICAL MODEL FOR INCREMENTAL DYNAMIC ANALYSIS

The calibrated numerical modelling procedure presented in the previous section was used to model additional field conditions in order to develop a database of results to investigate the effects of ground motion duration on the contribution of inertial and kinematic loads to the pile demands. The model was subjected to a suite of 12 short- and long-duration time histories spectrally matched to three different levels of shaking (36 motions). Each ground motion was applied under three different loading conditions (with/without liquefaction, and with/without deck inertial mass) to quantify the relative contribution of each load. The following sections describe the modifications to the numerical model, employed ground motions, and the loading conditions.

3.1 Modifications to Numerical Model

The calibrated numerical model was used to specifically model the centrifuge test, with several requirements that do not represent real field conditions (e.g., the centrifuge container). The model was modified for the incremental dynamic analysis in this study to better replicate field conditions by removing the centrifuge container walls and replacing them with free-field boundaries. The right and left boundaries of the model were extended to minimize the boundary effects on the cyclic response of the soil adjacent to the wharf. A rock layer with a shear wave velocity (Vs) of 760 m/s was added to the base of the model, and input ground motions were applied as outcrop motions using the compliant-base procedure of Mejia and Dawson (2006). The pile properties were changed to inelastic behavior with a bending moment capacity of 600 kN-m to represent the target prestressed concrete piles that are typically used in marginal wharves with similar geometries. Fig. 5 shows the modified *FLAC* model used in the incremental dynamic analysis. The calibration of the numerical model against centrifuge test ensures that the complex interaction between soil, pile and wharf is reasonably captured. The modifications applied to the boundaries to represent field conditions (e.g., the application of free-field conditions on the far left and far right boundaries and the use of compliant-base procedure to apply the input motions) are commonly-used approaches that have been used and validated by various studies (e.g., Mejia and Dawson 2006, Paull et al. 2022).

3.2 Input Ground Motions

The ground motions included a set of 12 shallow crustal and subduction earthquake time series covering a wide range of significant duration ($D_{5\text{-}95}$ ranging from 5 sec to 80 sec). Details of the input motions are provided in Table 3. The significant duration ($D_{5\text{-}95}$) is used in this study as a simple indicator to differentiate short-duration shallow crustal earthquakes from long-duration subduction earthquakes. Additionally, Arias Intensity (I_a) is used to investigate the combined effects of motion duration and amplitude on the interaction of inertial and kinematic demands. Arias Intensity, and other intensity measures that incorporate both amplitude and duration of acceleration (e.g., CAV_5), have been shown to be a good indicator of liquefaction effects on structures (e.g., Kramer and Mitchell 2006, Dickenson et al. 2014, Bullock et al. 2021). The motions were spectrally matched; therefore, the inertial demands were relatively constant among the 12 motions. However, the varying durations provided different kinematic demands.

The motions were first spectrally matched to the risk-targeted, maximum considered earthquake (MCE_R) spectrum developed using the site-specific ground motion procedures by ASCE 7-16 which is used as the basis for the Design Earthquake spectrum of ASCE 61-14 for a site located approximately 100 km from a major subduction zone (e.g., Portland, Oregon, where the seismic hazard includes significant contributions from the long-duration motions produced by a M 9.0 subduction zone earthquake). The MCE_R seismic hazard level is representative of ground motions having a 2% probability of exceedance in 50 years (i.e., 2,475-year average return period). These motions are indicated as "IDA 1.0" in subsequent plots. The spectrally matched motions were then linearly scaled by factors of 0.6 (IDA 0.6) and 1.5 (IDA 1.5). The scaled ground motions in IDA 0.6 represent the 975-year return period level of shaking which is approximately equal to the Design Earthquake spectrum per ASCE 61-14. The scaled ground motions in IDA 1.5 were used to impose larger inelastic demands on the piles to evaluate the effects of pile inelasticity on the interaction of inertial and kinematic demands. The IDA 1.5 motions are significantly larger than the IDA 1.0 ground motions to represent a site approximately 10 km away from a major subduction zone (e.g., along the coast of Oregon or Washington near the Cascadia Subduction Zone); therefore, the IDA 1.5 motions are considered relevant in evaluating the performance of port structures located closer to a subduction zone source. Acceleration response spectra for the three levels of dynamic shaking along with the time histories of the spectrally matched motions are shown in Fig. 6. The selected seed motions were rock motions with *Vs* greater than 570 m/s (with the exception of CHB002 which corresponds to a *Vs* of 360 m/s). Using the probability of pulse motions per Hayden et al. (2014), two of the four selected crustal motions contained velocity pulses. Additional details on the selection of ground motions and the matching process are provided in Khosravifar and Nasr (2017). It should be noted that while significant duration ($D_{5\text{-}95}$) is used in subsequent plots as an indicator of motion duration, specifically in the case of 2011 Tohoku motions, significant duration is a poor indicator of significant energy due to multiple sections of strong shaking that may be separated in time as shown by Walling et al. (2018).

3.3 Loading Conditions

Each nonlinear dynamic analysis was performed for three loading conditions, as illustrated in Fig. 7. Case A represents the full combination of inertial and kinematic loads, in which liquefaction-induced soil displacements apply kinematic lateral loads on the piles and where the deck mass applies inertial loads during shaking. In Case B, which considers only the inertial load, the loose sand was modeled as nonliquefiable by setting the contraction and dilation parameters in the PDMY03 model equal to zero. In this case, the excess pore pressure generation was precluded, and the model was subjected to minimal kinematic loads. Note that the term kinematic is used in this paper to refer to liquefaction-induced kinematic loads. For Case C, in which only the kinematic loads are considered, the inertial effects of the wharf deck were precluded by assigning the mass of the deck to zero. The soil parameters in Case C were kept the same as those in Case A. Note that the term inertia is used in this paper to refer to the deck inertial load.

4.0 RESULTS OF INCREMENTAL DYNAMIC ANALYSIS

The spectrally matched motions were used in the incremental dynamic analysis, in which the intensity of ground motions was increased linearly by three different scale factors (creating a total of 36 input motions) to provide varying levels of inelastic demands in piles. Each input motion was used in three loading conditions (inertial and kinematic, inertial only, kinematic only) creating a total of 108 dynamic analyses. The results of these analyses provide insights into the relative contributions of the inertial and liquefaction-induced kinematic loads on the overall demands on the pile-supported wharf as described in the following sections. However, it should be noted that the interaction of inertia and kinematics is a complex and nonlinear dynamic problem. The timing, rate, and onset of significant soil softening due the progressive increase in excess pore pressure affect the dynamic response of the soil profile. Therefore, the magnitude of the inertial demand in the liquefied condition is different from that in the nonliquefied condition. Nevertheless, analyzing the nonliquefied case provides a reasonable estimate of the inertial load–induced demands that are frequently considered in pile design.

4.1 Free-field Site Response

Acceleration time histories were extracted from the model at the ground surface far away from the structure to represent the free-field response and were used to calculate the acceleration response spectra for a 5% damping ratio. Acceleration response spectra and the corresponding soil amplification ratios at the ground surface are plotted in Fig. 8 for the loading cases with liquefaction (Case A which is identical to Case C in terms of free-field site response) and without liquefaction (Case B). The soil amplification ratios were computed as the ratio of the acceleration response spectra at the ground surface to the outcrop spectra at the base of the model. The response spectra correspond to the computed horizontal acceleration at the ground surface at a location far away from the wharf (at a distance of 40 meters) as shown by a circle symbol in the schematic in Fig. 8a. The results in this figure are shown for the ground motions in IDA 1.0 (matched to the MCE_R level spectra) as an example. The median PGA is approximately 0.4 g in the nonliquefied condition, and it drops to approximately 0.2 g in the liquefied condition. The spectral accelerations for periods shorter than 1 sec in liquefied condition are noticeably smaller than those where liquefaction is absent. The mean amplification curve in the absence of liquefaction shows that, on average, the maximum amplification occurred at a period of approximately 0.6 sec. In the condition with liquefaction, the maximum amplification occurred at periods greater than 1 sec due to the softening effects from liquefaction. These periods correspond to the fundamental period of the soil profile in the free-field. While some case histories presented by Youd and Carter (2005) show amplification of long period motions due to liquefaction, the amplification factors less than 1 for long periods (>3 sec) in liquefied conditions for the specific geometry and subsurface conditions analyzed here are within the range predicted by Gingery et al. (2014) for large magnitude earthquakes.

4.2 Effects of Liquefaction on Peak Kinematic Demands

Figure 9 shows the variation of peak horizontal ground displacement with significant duration of the input motions, $D_{5\text{-}95}$ (Fig. 9a), the peak base acceleration (Fig. 9b), and Arias Intensity (Fig. 9c). The displacements correspond to the ground surface at the backland relative to the base of the model. The plotted data include the results of the analyses performed for the liquefied conditions (Case A) and nonliquefied conditions (Case B) for all ground motions in the incremental dynamic analyses. Fig. 9a shows that, as expected, the peak ground displacements (and the corresponding kinematic effects) are significantly larger under liquefied conditions as compared to nonliquefied conditions. The peak ground displacements in the liquefied condition are positively correlated with ground motion duration. As anticipated, this finding indicates that while all the ground motions were spectrally matched, the soil profile incrementally accumulated more shear strain in long-duration motions. In contrast, the nonliquefied cases show relatively little correlation with motion duration; this is expected, as all the ground motions were spectrally matched to the same target spectra and the slope configuration in this study did not yield in nonliquefied conditions under the applied seismic demands. It is worth noting that the yield acceleration of the slope analyzed here is approximately 0.57 g using limit equilibrium analysis and nonliquefied soil properties, which is larger than the PGA of the input motions. The variations in the peak ground displacements for a given motion duration shown in Fig. 9a are attributed to the varying intensity of the input motions. As revealed from the plot in Fig. 9c, the peak ground surface displacements increase with the Arias Intensity of the input motion under both liquefied and nonliquefied conditions. The peak ground surface displacements in liquefied case are between 4 to 12 times larger than those in nonliquefied conditions over the range of Arias Intensity values covered in this study.

4.3 Effects of Liquefaction on Peak Inertial Demands

As shown earlier in Fig. 8, the spectral accelerations at the ground surface are smaller in the liquefied conditions as compared to nonliquefied conditions, particularly over the effective fundamental periods of the soil-wharf system ranging from 0.9 sec in nonliquefied conditions and 1 sec in liquefied conditions (these periods are estimated based on the effective secant stiffness estimated from nonlinear static pushover analysis following the procedures in ASCE 61-14). According to Fig. 8, the spectral accelerations at the mentioned period of 1 sec reduced from approximately 0.5 g in nonliquefied conditions to approximately 0.3 g in liquefied conditions (i.e. a reduction factor of 0.6 due to soil liquefaction.) Therefore, it is expected that the peak inertial loads are also reduced due to liquefaction. Fig. 10 shows the ratio of the peak wharf accelerations in liquefied conditions (Case A) to that for nonliquefied conditions (Case B). This ratio is denoted as C_{liq} in this figure and is plotted against; (a) significant duration, $D_{5\text{-}95}$, (b) peak base acceleration, and (c) Arias Intensity. For a majority of the cases, the C_{liq} ratio is below one, indicating that the peak inertial demands produced in liquefied conditions are smaller than those in the absence of liquefaction. The C_{liq} shows a slightly increasing trend with motion duration, a slightly decreasing trend with peak base acceleration, and no significant change with Arias Intensity. The C_{liq} values calculated in this study range from 0.7 to 1.1 with mean value of 0.85.

For comparison, the C_{liq} values reported by Boulanger et al. (2007) from a series of centrifuge tests for highway bridge foundations range from 0.35 to 1.4 and the C_{liq} values calculated from the results of a series of shake table tests by Tokimatsu et al. (2005) range from 0.2 to 0.3. The wide range of liquefaction effects on peak inertial loads observed in this study and reported in the literature highlights the influence of geometry, stratigraphy, and the complexity of liquefaction on soil–foundation–structure behavior. These complex behaviors also affect the timing of liquefaction triggering with respect to the timing of peak inertia as discussed in the next section.

4.4 Timing of Liquefaction and Peak Inertia

As described in the previous section, the effects of liquefaction on inertial demands depend on the timing of liquefaction triggering and peak inertial loads — which, in turn, are influenced by the characteristics of input motion, the rate of pore pressure generation, and subsequent development of kinematic loads. These effects are discussed in this section with respect to ground motion duration. The dynamic response of the soil and wharf are plotted in Fig. 11 for two motions that are spectrally matched to the MCE_R spectra but have significantly different durations. The short-duration, shallow crustal motion corresponds to the 1992 Cape Mendocino earthquake (CPM station) and the long-duration subduction motion corresponds to 2011 Tohoku earthquake (MYGH06 station). Fig. 11 shows the representative time histories of ground surface displacement, wharf deck acceleration and displacement, and excess pore pressure ratio (r_u) in the middle of the loose sand layer (used here to indicate the triggering of liquefaction). The time of the peak response is marked in each plot with a vertical dashed line and a triangle. In the short-duration motion (CPM), the peak wharf acceleration occurred prior to the triggering of liquefaction (3.5 sec versus 9.5 sec.) However, in the long-duration motion (MYGH06), the peak wharf acceleration occurred after liquefaction was triggered (68 sec versus 24 sec). It is also noticeable that while the ground displacements in the long-duration motion continued to accumulate following the triggering of liquefaction and reached a peak value at around 78 sec, those in the short-duration motion did not increase further after liquefaction was triggered. These behaviors are indicative of cyclic mobility and the accumulation of shear strains during cyclic loading. This phenomenon is different than the flow liquefaction reported in other studies, where large lateral spreading displacements develop towards the end of motion due to instability of the slope under a static shear stress. It is also important to note that the peak deck displacements are heavily correlated with the peak soil displacements in both motions for the relatively flexible piles in this study (the relative stiffness factor (T) for the piles in this study is 2.1 using $T= (EI/k)^{(1/5)}$ where EI is the flexural stiffness of the pile and k is the subgrade reaction for rockfill). In the cases analyzed here, the piles tend to closely follow the soil displacements. This behavior may be different when considering relatively stiff piles, such as large-diameter shafts that are not typically used for pile-supported wharves, but are often used in highway bridges.

The observations from the example motions in Fig. 11 are summarized for all motions analyzed in this study in Fig. 12, where the relative timing of the peak inertial load (indicated by the wharf deck acceleration) is plotted against the timing of liquefaction triggering and the timing of maximum ground displacement. Fig. 12a shows that the majority of the long-duration motions (those having a $D_{5\text{-}95}$ greater than 26 sec) fall close to or above the 1:1 line, which indicates that peak wharf acceleration occurred after the triggering of liquefaction. In contrast, in short-duration motions, the peak wharf acceleration occurred prior to the triggering of liquefaction.

While it is important to consider the timing of liquefaction triggering, it is equally important to consider the timing of the peak ground displacements, as it was shown in the example time histories in Fig. 11 that the timing of maximum demands on the piles (i.e., peak wharf deck displacement) is highly correlated with the timing of maximum ground displacements. Fig. 12b shows that the maximum wharf accelerations occurred before the ground displacements reached their peak values in all motions studied here (both short- and long-duration motions). This is important, as it will be shown later, that for relatively flexible piles the wharf and pile behaviors are dominated by the large ground displacements that develop in long-duration motions.

4.5 Contribution of Inertial Load During the Critical Cycle

The time of peak inertial load does not necessarily coincide with the time of the critical cycle when the pile demands are at their peak values particularly when the kinematic loads are large. The relative contribution of the peak inertial load during the critical cycle is characterized in this section using the normalized wharf deck acceleration (acceleration at time *t* divided by the peak wharf acceleration) at the critical cycle. Most design codes use pile bending moments (and strains) as the primary engineering parameter to characterize the pile performance (e.g., strain limits for different target performance levels defined in ASCE 61-14). Therefore, the critical cycle is defined in this study as the time when the bending moments are at their peak value. To calculate the wharf acceleration ratios, first, key locations where large bending moments developed among all piles were determined. The locations of large bending moments were generally located at the connection of pile head and the wharf deck, near the boundary between rockfill and loose sand, and near the boundary between loose sand and lower dense sand. Then, the wharf accelerations were extracted at the time when the bending moment in each key location was at the peak value (the maximum bending moments did not necessarily occur at the same time in all locations). Finally, the extracted wharf accelerations were normalized by the peak wharf acceleration.

Figure 13 shows the wharf acceleration ratios at the critical cycle versus strong motion duration (Fig. 13a) and Arias Intensity (Fig 13.b). For plotting purposes, only the average of all acceleration ratios is plotted for each ground motion in this figure. The data is shown for different IDA values to illustrate the correlations between the acceleration ratios and motion duration (i.e. $D_{5\text{-}95}$) and motion amplitude (i.e. different IDA values). The relationship with Arias Intensity, which includes the combined effect of motion duration and motion amplitude, is shown in Fig. 13b. This figure shows a slightly increasing trend with motion duration and Arias Intensity. For example, for IDA 1.0 (corresponding to MCE_R level motions), the mean inertial ratios increase from 0.6 for short-duration crustal earthquakes (with $D_{5\text{-}95}$ < 20 sec) to 0.76 for long-duration subduction earthquakes (with $D_{5\text{-}95}$ > 20 sec) indicating that there is a larger likelihood for peak deck acceleration to interact constructively with peak kinematic loads during long-duration motions compared to short-duration motions. Similarly, the mean inertial ratios increase from 0.6 for motions with small Arias Intensity (I_a < 3 m/s) to approximately 0.75 for motions with large Arias Intensity (I_a > 3 m/s). The increasing trend between acceleration ratios and Arias Intensity is attributed to larger ductility demands in piles. A similar trend was reported in Khosravifar et al. (2014) where inertial contribution factors were found to increase with larger ductility demands in piles.

For comparison, data from three centrifuge tests with very similar geometries and properties to the wharf modeled here are plotted in this figure. NJM01 was used in the calibration of the numerical model. Additional details on NJM02 and SMS01 can be found in Schlechter et al. (2000a,b) and the back-calculation of the inertial load factors from centrifuge tests are provided in Souri (2021). For the short-duration motions (those with a $D_{5\text{-}95}$ shorter than 20 sec), the *FLAC* simulations suggest acceleration ratios ranging between 0.45 to 0.85, which are within the range observed in the three centrifuge tests. The computed acceleration ratios in Fig. 13 are also comparable to the C_{cc} values recommended by Boulanger et al. (2007), which range from 0.65 to 0.85 as marked by the hatched area in Fig. 13. C_{cc} is defined as the fraction of the maximum inertial load with liquefaction that occurs at the critical loading cycle. As described earlier, the critical cycle is defined in this study as the time when the peak bending moment occurs during the ground motion. Despite a slightly larger likelihood of inertia and kinematic interaction in long-duration motions, it will be shown later that for small-diameter flexible piles, this interaction becomes less relevant to the design of the piles as the magnitude and influence of kinematic loads on relatively flexible piles become significantly larger than the inertial contribution in long-duration motions.

4.6 Contribution of Inertial and Kinematic Demands on Overall Wharf Response

The relative contribution of inertial and kinematic demands on the overall wharf response was evaluated by performing the incremental dynamic analyses for the three load conditions previously defined in Fig. 7.

In Fig. 14, the maximum wharf deck displacements in the three loading conditions are compared against input motion duration and Arias Intensity. As indicated by the fitted curves shown by the dashed lines for IDA 0.6, 1.0 and 1.5 in Fig. 14, the maximum pile demands in liquefied cases (with or without inertial loads) increase steeply with the duration of motion and Arias Intensity, whereas the maximum pile demands in the nonliquefied case (deck inertia only) show no correlation with motion duration and much flatter correlation with Arias Intensity. This is somewhat expected, considering that the ground motions used in these analyses are spectrally matched to the same target spectra; thus, exerting the same amount of inertial force on the wharf deck. As noted previously, the imposed demands on the slope did not exceed the yield acceleration in nonliquefied conditions. For the short-duration motions, the pile demands under combined case are larger but comparable to the demands under inertia only and kinematic only cases. In contrast, for long-duration motions, the pile demands in the combined case are much larger than the inertia only demands and are primarily governed by the liquefaction-induced kinematic demands. This finding suggests that despite the higher likelihood of interaction between the inertial and kinematic loads in long-duration motions (as shown previously in Fig. 13), the contribution of the inertial loads in the overall demands is much smaller, and the kinematic demands seem to govern the design. This finding may be considered in the assumptions that need to be made in combining the inertial and kinematic demands when designing for short-duration or long-duration events.

The data in Fig. 14 are replotted in Fig. 15 to provide more insight on the relative contribution of inertial and kinematic loads in the overall demands on the wharf. The horizontal axes in Figs. 15a and 15b show the maximum deck displacements under the combined effects of inertial and kinematic loads (Case A). The vertical axes in Figs. 15a and 15b show the maximum deck displacements under inertial loads only (Case B) and under kinematic loads only (Case C), respectively. Fig. 15a shows that the maximum deck displacements could be significantly underpredicted (by an average factor of 0.33) by considering only the inertial effects in the absence of liquefaction. Fig. 15b shows that the maximum deck displacements could be slightly underpredicted (by an average factor of 0.9) by considering only the kinematic effects.

Figs. 15c to 15f show the variation of data points in the left two plots with respect to motion duration and Arias Intensity. The horizontal axes in Figs. 15c and 15d show the significant duration of input motion $D_{5\text{-}95}$ and Arias Intensity. The vertical axes in these figures show the ratio of maximum deck displacements in the inertia only (Case B) or kinematics only (Case C) versus those considering combined inertial and kinematic loading (Case A). Figs. 15c and 15e show that as the motion duration and intensity increase, the contribution of inertial loads to the overall wharf demands decreases. On the other hand, Figs. 15d and 15f show that the contribution of kinematic loads on the overall wharf demands slightly increases with motion duration and intensity though this amount is insignificant considering other uncertainties in estimating seismic demands in design. The response of the wharf structure modeled here is heavily influenced by kinematic demands, as the relatively flexible piles tend to follow the pattern of ground deformations; these deformations increase with motion duration such that in long-duration motions, the wharf demands become primarily governed by kinematic loads and less so by inertial loads. This response may be different for stiffer piles (e.g., large-diameter pile shafts that are typically used for highway bridge structures), where the kinematic loads on piles do not increase further once the relative displacements between the pile and soil exceed a certain value required to mobilize full lateral passive pressure on piles.

The relative contribution of inertial and kinematic demands for a wharf subjected to short- and long-duration motions is examined further using the two IDA 1.0 motions shown in Fig. 16. The time histories of the wharf deck displacements are plotted for the combined inertial and kinematic loads (Case A) as well as for inertia only (Case B) and kinematics only (Case C) and are compared for a short-duration motion (CPM) and a long-duration motion (MYGH06). The magnitude of maximum deck displacements under inertial load only (Case B) are similar in both motions (i.e. 0.09 m), as both motions are spectrally matched to MCE_R spectra. The wharf displacements under kinematic load only (Case C) closely follow the pattern in the combined case (Case A) in both motions. However, the magnitude of displacements in Cases C and A are much larger for the long-duration motion than for the short-duration motion. As shown in the time histories for the long-duration motion, the structure continues to experience strong inertial cycles throughout the motion (note the large inertial cycles at around 70 sec), however the relative contribution of these loads becomes less significant as the kinematic demands begin to dominate the wharf response.

5.0 CONCLUDING REMARKS

The main objective of this study was to investigate the potential differences between the interaction of inertial and liquefaction-induced lateral spreading loads during short-duration crustal earthquakes and long-duration subduction earthquakes for a typical pile-supported wharf structure. The interaction of inertial and kinematic loads and their contribution to the overall demands on piles were evaluated with respect to ground motion intensity measures that are commonly used in engineering practice; strong motion duration ($D_{5\text{-}95}$) and Arias Intensity (I_a). A two-dimensional numerical model of a pile-supported wharf was used in nonlinear dynamic analyses. The 2D model was calibrated using a recently re-evaluated set of data from a large-scale centrifuge test. The dynamic performance of the pile supported wharf was simulated using a suite of spectrally matched ground motions with varying motion durations to evaluate the relative contribution of inertial and kinematic loads on the response of the wharf. The analyses were performed for three loading conditions including combined effects of inertial loads from the wharf deck and kinematic ground deformations (Case A), deck inertial load in the absence of liquefaction with minimal kinematic demands (Case B), and kinematic load in the absence of deck mass (Case C). The primary conclusions of the study are summarized as follows:

- As shown in Fig. 15, wharf deck displacement demands are mostly governed by kinematic demands. The combined effects of inertial and kinematic loads (Case A) were, on average, 3 times larger than the demands due to inertial loads only (Case B), whereas the deck displacements in the combined case (Case A) were only, on average, 1.1 times larger than the case involving kinematic loads only (Case C).
- It was recognized that the response of the wharf supported on relatively flexible piles was largely influenced by lateral soil displacements. As shown in Fig. 9, the lateral soil displacements were found to be well correlated with motion duration and intensity due to accumulation of shear strain in liquefied soil in many loading cycles. Consequently, the wharf demands were found to be strongly correlated with motion durations and intensity for the spectrally matched ground motions with almost identical response spectra.
- The wharf demands (i.e., deck displacements) in nonliquefied conditions were primarily driven by the inertial loads from the deck mass with minor variation due to motion duration for the spectrally matched motions used in this study. This was due,

in large part, to the small seismically-induced slope deformations computed for the inertia only cases.

- For the wharf structure modeled in this study, the occurrence of liquefaction reduced the peak inertial load from the wharf deck in most cases (C_{liq} parameters ranged from approximately 0.7 to 1.1 as shown in Fig. 10) and showed a slightly increasing trend with motion duration, a slightly decreasing trend with peak base acceleration, and no significant correlation with Arias Intensity.

- The analyses in this study suggest that the likelihood of inertial load interacting with kinematic load (characterized by the ratio of inertial load at the critical cycle to the peak inertial load during the entire motion) increased with motion intensity and motion duration. Up to 15% increase was observed in the inertial contribution factors between short-duration crustal motions and long-duration subduction motions for ground motions that were spectrally matched to MCE_R level shaking. Similarly, an approximately 15% increase was observed in the inertial contribution factors between motions with small Arias Intensity (I_a <3 m/s) compared to motions with large Arias Intensity (I_a >3 m/s). However, it was found that the dynamic and residual loads in the piles characteristic of those used at ports in the western United States were heavily influenced at critical depths by the kinematic loads in long duration motions resulting in significant slope deformation and less so by the inertial loads.

- The Arias Intensity (I_a) was generally found to be a better predictor for peak ground and peak deck displacements compared to strong motion duration ($D_{5\text{-}95}$) and input acceleration amplitude (PGA).

The approach used in this study consisted of calibrating a numerical model to a well-instrumented centrifuge test involving a short duration earthquake and using the validated modelling procedure to model a typical pile-supported wharf for both short and long duration earthquakes. The calibration study provided an important benchmark for the subsequent study to investigate the contribution of inertial and kinematic loads on overall pile demands with respect to selected ground motion intensity measures (i.e., significant duration and Arias Intensity). The suitability of this approach is supported by results of concurrent investigations in which the soil constitutive model used in this study performs equally well for simulation of permanent displacements of slopes subjected to short duration and long duration earthquakes, when calibrated properly to produce the desired cyclic resistance relationship (i.e., CRR versus number of uniform loading cycles). The application and further refinement of practice-oriented inertial and kinematic load factors will benefit from additional research expanding this analysis to a broader array of waterfront structures and soil conditions.

6.0 ACKNOWLEDGEMENTS

Support for conducting centrifuge tests was provided by Grant No. CMS-9702744 from the National Science Foundation (NSF) and Grant No. SA2394JB from the Pacific Earthquake Engineering Research Center (S. Dickenson, P.I.). Support for recent analyses of the centrifuge tests was provided by Grant No. CMMI-1761712 from NSF and Grant No. 171126 from the Deep Foundations Institute (A. Khosravifar, P.I.). Any opinions, findings, and conclusions or recommendations expressed in this article are those of the author(s) and do not necessarily reflect the views of the funding agencies.

7.0 REFERENCES

AASHTO (American Association of State Highway and Transportation Officials) (2014). *Guide Specifications for LRFD Seismic Bridge Design*. 2nd ed. with 2014 Interim. Washington, DC:

Abdoun, T., and Dobry. R. (2002). Evaluation of pile foundation response to lateral spreading. Soil Dyn. and Earthq. Eng. 22: 1051–1058.

Abdoun, T., Dobry, R., O'Rourke, T.D., and Goh, S.H. (2003). Pile response to lateral spreads: centrifuge modeling. J. of Geotech. and Geoenv. Engineering, 129(10), 869-878.

API (American Petroleum Institute) (1993). Recommended practice for planning, design, and constructing fixed offshore platforms, 20th ed. API RP 2A-WSD. Washington, DC.

ASCE (American Society of Civil Engineers) (2014). *Seismic Design of Piers and Wharves,* ASCE/COPRI 61-14. ASCE Standards Committee on Seismic Design of Piers and Wharves. Reston, Va.: ASCE. https://doi.org/10.1061/9780784413487.

Ashford, S., Boulanger, R., and Brandenberg, S. (2011). Recommended Design Practice for Pile Foundations in Laterally Spreading Ground. Report PEER 2011/04, Pacific Earthquake Engineering Research Center (PEER), Berkeley, CA.

Bentley, K. J., & Naggar, M. H. E. (2000). Numerical analysis of kinematic response of single piles. Canadian Geotechnical Journal, 37(6), 1368-1382.

Boulanger, R. W., Curras, C. J., Kutter, B. L., Wilson, D. W., & Abghari, A. (1999). Seismic soil-pile-structure interaction experiments and analyses. *Journal of geotechnical and geoenvironmental engineering*, *125*(9), 750-759.

Boulanger, R. W., Chang, D., Brandenberg, S. J., Armstrong, R. J., and B. L. Kutter (2007). Seismic design of pile foundations for liquefaction effects. In *Proc. of 4th International Confer. on Earthquake Geotechnical Engineering*, 277–302. Dordrecht, Germany: Springer.

Boulanger, R. W., Khosravi, M., Khosravi, A., & Wilson, D. W. (2018). Remediation of liquefaction effects for an embankment using soil-cement walls: Centrifuge and numerical modeling. *Soil Dynamics and Earthquake Engineering*, *114*, 38-50.

Brandenberg, S. J., Zhao, M., Boulanger, R. W., & Wilson, D. W. (2013). p-y plasticity model for nonlinear dynamic analysis of piles in liquefiable soil. Journal of geotechnical and geoenvironmental engineering, 139(8), 1262-1274.

Bullock, Z., Liel, A. B., Dashti, S., & Porter, K. A. (2021). A suite of ground motion prediction equations for cumulative absolute velocity in shallow crustal earthquakes including epistemic uncertainty. *Earthquake Spectra*, *37*(2), 937-958.

California Department of Transportation (Caltrans) (2012). *Guidelines for Foundation Loading and Deformation Due to Liquefaction Induced Lateral Spreading*. Sacramento, CA: Caltrans.

California Department of Transportation (Caltrans) (2016). Lateral Spreading Analysis for New and Existing Bridges. Memo to Designers 20-15, Sacramento, CA.

Chopra, A. K. (1995). Dynamics of Structures: Theory and Applications to Earthquake Engineering, Prentice Hall. *Inc., Upper Saddle River, NJ*.

Cubrinovski, M., Bray, J. D., de la Torre, C., Olsen, M. J., Bradley, B. A., Chiaro, G., Stocks, E. and L. Wotherspoon (2017). Liquefaction effects and associated damages observed at the Wellington Centreport from the 2016 Kaikoura earthquake." *Bull. N. Z. Soc. Earthq. Eng*., 50 (2): 152–173.

Cubrinovski, M., and K. Ishihara (2006). Assessment of pile group response to lateral spreading by single pile analysis. In *Seismic Performance and Simulation of Pile Foundations in Liquefied and Laterally Spreading Ground*, GSP 145, 242–254. Reston, Va.: ASCE.

Dickenson, S., Yang, S., Schwarm, D., and Rees, M. (2014). Seismic performance analysis of pile-supported wharves subjected to long-duration ground motions. In *SMIP14 Proceedings of Seminar on Utilization of Strong-Motion Data, Los Angeles, California* (pp. 63-82).

Dobry, R., Abdoun, T., O'Rourke, T. D., and S. H. Goh (2003). Single piles in lateral spreads: Field bending moment evaluation. *J. Geotech. Geoenviron. Eng.* 129, 879–889.

Donahue, M. J., Dickenson, S. E., Miller, T.H., and Yim, S.C. (2005). Implications of the Observed Seismic Performance of a Pile Supported Wharf for Numerical Modeling. Earthquake Spectra, EERI, 21(3), 617-634.

Egan, J. A., and Wang, Z. L. (1991). Liquefaction-related ground deformation and effects on facilities at Treasure Island, San Francisco, during the 17 October 1989 Loma Prieta Earthquake. In Proc. of the 3rd Japan–US workshop on earthquake resistant design of lifeline facilities and countermeasures for soil liquefaction. NCEER-91–0001 (pp. 57–76).

El Naggar, M. H., & Novak, M. (1996). Nonlinear analysis for dynamic lateral pile response. Soil Dynamics and Earthquake Engineering, 15(4), 233-244.

Electric Power Research Institute (EPRI) (1990). Manual on Estimating Soil Properties for Foundation Design. Electric Power Research Institute, Palo Alto, California, 308 pp.

Finn, W. D. L. (2005). A study of piles during earthquakes: Issues of design and analysis. *B. Earthq. Eng.*, 3(2), 141–234. https://doi.org/10.1007/s10518-005-1241-3

Gazetas, G., & Dobry, R. (1984). Simple radiation damping model for piles and footings. *Journal of Engineering Mechanics*, *110*(6), 937-956.

Gingery, J. R., Elgamal, A., & Bray, J. D. (2015). Response spectra at liquefaction sites during shallow crustal earthquakes. Earthquake Spectra, 31(4), 2325-2349.

Hayden, C. P., Bray J. D. and Abrahamson, N. A. (2014). Selection of near-fault pulse motions. Journal of Geotechnical and Geoenvironmental Engineering, 140(7), 04014030.

Idriss IM, Boulanger RW. (2008). Soil liquefaction during earthquakes. Monograph. MNO-12. Oakland, CA: Earthquake Engineering Research Institute; [261p].

Itasca (2016). FLAC, Fast Lagrangian Analysis of Continua, User's Guide, Version 8.0. Minneapolis, MN: Itasca Consulting Group, Inc.

Khosravifar, A., Boulanger, R. W. and Kunnath, S. K. (2014). Effects of liquefaction on inelastic demands on extended pile shafts. Earthquake Spectra, 30(4), 1749–1773.

Khosravifar, A., Elgamal, A., Lu, Jinchi, Li, John (2018). A 3D model for earthquake-induced liquefaction triggering and post-liquefaction response. Soil Dynamics and Earthquake Engineering, 110, pp. 43–52

Khosravifar, A. and Nasr, J. (2017). Modified design procedures for bridge pile foundations subjected to liquefaction-induced lateral spreading. *DFI Journal-The Journal of the Deep Foundations Institute*, *11*(2-3), pp.114-127.

Kramer, S.L. and Mitchell, R.A. (2006). Ground motion intensity measures for liquefaction hazard evaluation." *Earthquake Spectra*, *22*(2), pp.413-438.

Kutter, B. L. (1992). Dynamic centrifuge modeling of geotechnical structures. *Transportation research record*, (1336).

Lambe, T. W. (1973). Predictions in soil engineering. *Géotechnique*, *23*(2), 151-202.

Makris, N., & Gazetas, G. (1992). Dynamic pile-soil-pile interaction. Part II: Lateral and seismic response. Earthquake engineering & structural dynamics, 21(2), 145-162.

Martin, G. R., March, M. L., Anderson, D. G., Mayes, R. L., and M. S. Power (2002). Recommended design approach for liquefaction induced lateral spreads. In *Proc. of 3rd National Seismic Conf. on Bridges and Highways*, MCEER-02-SP04, Buffalo, N.Y.

McCullough, N.J., S.E. Dickenson, B. L. Kutter, and D.W. Wilson (2000). *Pile-Supported Wharf — Centrifuge Model NJM01. Report No. GEG01-2000*. Oregon State Univ./UC Davis.

McCullough, N., and S. Dickenson (2004). The Behavior of Piles in Sloping Rock Fill at Marginal Wharves. In *Proc. Ports Conference 2004*, Reston, VA: ASCE.

McCullough, N. J., S. E. Dickenson, and S. M. Schlechter (2001). The seismic performance of piles in waterfront applications." In *Ports Conference 2001*, 1–10. Reston, VA: ASCE.

McCullough, N. J., S. E. Dickenson, and S. M. Schlechter. J. C. Boland (2007). Centrifuge Seismic Modeling of Pile-Supported Wharves. Geotechnical Testing Journal, Vol. 30, No. 5

MCEER (Multidisciplinary Center for Earthquake Engineering Research) (2003). *Recommended LRFD Guidelines for the Seismic Design of Highway Bridges.* MCEER/ATC-49, Report No. MCEER-03-SP03. Buffalo, N.Y.: University at Buffalo.

Mejia, L. H. and Dawson, E. M. (2006). Earthquake deconvolution for FLAC. Proceedings of fourth international FLAC symposium on numerical modeling in geomechanics, Madrid.

Morales, C., Ledezma, C., Sáez, E., Boldrini, S., & Rollins, K. (2020). Seismic failure of an old pier during the 2014 Mw8. 2, Pisagua, Chile earthquake. Earthquake Spectra, 36(2), 880-903.

ODOT (Oregon Department of Transportation) (2014). *Geotechnical Design Manual.* Tech. Services Branch, Salem, OR

Olson, S.M., Hashash, Y.M.A., Muszynski, M.R., and Phillips, C. (2017). Passive wedge formation and limiting lateral loads on large foundations during lateral spreading. ASCE Journal of Geotechnical and Geoenvironmental Engineering, 143(7), 13p.

Paull, N. A., Boulanger, R. W., DeJong, J. T., & Friesen, S. J. (2022). Nonlinear Dynamic Analyses of Perris Dam Using Transition Probability to Model Interbedded Alluvial Strata. Journal of Geotechnical and Geoenvironmental Engineering, 148(1).

POA (Port of Anchorage) (2017). Anchorage Port Modernization Project Seismic Design Manual.

POLB (Port of Long Beach) (2015). Port of Long Beach Wharf Design Criteria. Version 4.0 (May). Long Beach, CA: POLB.

Seed, H. B., and Idriss, I. M. (1970). Soil moduli and damping factors for dynamic response analysis. Rep. No. UCB/EERC-70/10, Earthq. Engrg. Res. Ctr., Univ. of Calif. at Berkeley

Schlechter, S. M., McCullough, N. J., Dickenson, S. E., Kutter, B. L., and D. W. Wilson (2000a). *Pile-Supported Wharf — Centrifuge Model NJM02.* Report No. GEG02-2000, Oregon State University/University of California at Davis.

Schlechter S. M., McCullough, N. J., Dickenson, S. E., Kutter, B. L., and D.W. Wilson (2000b). *Pile-Supported Wharf — Centrifuge Model SMS01.* Report No. GEG03-2000, Oregon State University/University of California at Davis.

Shafieezadeh, A., DesRoches, R., Rix, G. J., & Werner, S. D. (2012). Seismic performance of pile-supported wharf structures considering soil-structure interaction in liquefied soil. *Earthquake Spectra*, *28*(2), 729-757.

Souri, M., Khosravifar, A., Schlechter, S., McCullough, N. and S. E. Dickenson (2020). Development of experimental p-y curves from centrifuge tests for piles subjected to static loading and liquefaction-induced lateral spreading. *DFI Journal* 14 (1), 1–15

Souri, M. (2021). Development of a Design Guideline for Pile Foundations Subjected to Liquefaction-Induced Lateral Spreading. PhD Dissertation, Portland State University. https://pdxscholar.library.pdx.edu/open_access_etds/5695/

Tokimatsu, K., and Y. Asaka (1998). Effects of liquefaction-induced ground displacements on pile performance in the 1995 Hyogoken-Nambu earthquake. *Soils Found.* 38 (suppl.): 163–177.

Tokimatsu, K. (2003). Behavior and design of pile foundations subjected to earthquakes. In *Proc. of 12th Asian Regional Conference on Soil Mechanics and Geotechnical Engineering*, 1065–1096. Klong Luang, Thailand: Association of Geotechnical Societies in Southeast Asia.

Tokimatsu, K., Suzuki, H., and M. Sato (2005). Effects of inertial and kinematic interaction on seismic behavior of pile with embedded foundation. *Soil Dyn. Earthq. Eng.* 25 (7-10):753-762.

Turner, B. J., Brandenberg, S. J., and J. P. Stewart (2016). Case study of parallel bridges affected by liquefaction and lateral spreading. *J. Geotech. Geoenviron. Eng.* 142.7 (2016): 05016001.

Vytiniotis A., Panagiotidou A.-I., Whittle A.J. (2019). Analysis of seismic damage mitigation for a pile-supported wharf structure. Soil Dyn Earthq Eng, 119 (2019), pp. 21-35

Walling, M., Kuehn, N., Abrahamson, N., & Mazzoni, S. (2018). Regional ground motion duration prediction model for subduction regions. In *11th US National confer. on earthq. engineering*.

Wang, S., Kutter, B.L., Chacko, M.J., Wilson, D.W, Boulanger, R.W., and A. Abghari (1998). Nonlinear Seismic Soil-Pile Structure Interaction. Earthquake Spectra 14(2): 377–396.

WSDOT (Washington Dept. of Transportation) (2021). Geotechnical Design Manual. M 46-03.14.

Youd, T. L., & Carter, B. L. (2005). Influence of soil softening and liquefaction on spectral acceleration. Journal of Geotechnical and Geoenvironmental Engineering, 131(7), 811-825.

Table 1. Pile, superstructure, and soil properties and ground motion in centrifuge test NJM01 (in prototype scale)

Pile properties	Superstructure properties	Soil properties	Applied ground motions at base
Pile diameter (D) = 0.64 m Wall thickness (t) = 0.036 m Length (L) = 27.2 m Flexural stiffness (EI) = 2.1e5 kPa-m^4 Out-of-plane spacing = 6.1 m	Wharf deck 33.7 m × 15.2 m × 0.25 m, mass = 714.8 Mg Out-of-plane spacing = 6.1 m	Nevada loose sand, D_R = 39% Nevada dense sand, D_R = 82% Rockfill, friction angle = 45 deg	Event 11 – 1989 Loma Prieta Outer Harbor Station scaled to peak ground acceleration (PGA) = 0.15g

Table 2. Soil properties in the PDMY03 constitutive model

Model parameters	Loose sand	Lower and upper dense sands	Rockfill
Relative density, D_R [a]	39%	82%	N.A.
Cyclic resistance ratio, $CRR_{\sigma'v=1, M=7.5}$ [a]	0.1	N.A.	N.A.
Density, ρ	1.94 Mg/m^3	2.04 Mg/m^3	2.05 Mg/m^3
Reference mean effective pressure, p'_r	101 kPa	101 kPa	101 kPa
$K_{2,max}$ [a]	38	65	100
Small-strain shear modulus at reference pressure, $G_{max, r}$	69.6 MPa	111.9 MPa	154.7 MPa
Maximum shear strain at reference pressure, $\gamma_{max, r}$	0.1	0.1	0.1
Bulk modulus at reference pressure, B_r	209 MPa	242.5 MPa	206.3 MPa
Pressure dependent coefficient, d	0.5	0.5	0.5
DSS Friction angle, φ_{DSS} [a]	33°	37°	45°
Model friction angle, φ	28.3°	32.4°	42.2°
Phase transformation angle, φ_{PT}	23.3°	27.4°	32.2°
Contraction coefficient, c_a	0.063	0.001	0.001
Contraction coefficient, c_b	5.0	0.5	0.5
Contraction coefficient, c_c	0.2	0.0	0.0
Contraction coefficient, c_d	0.0	0.0	0.0
Contraction coefficient, c_e	0.0	0.0	0.0
Dilation coefficient, d_a	0.15	0.4	0.4
Dilation coefficient, d_b	3.0	3.0	3.0
Dilation coefficient, d_c	0.0	0.0	0.0
Number of yield surfaces, NYS	20	20	20
S_0	1.73 kPa	1.73 kPa	13.0 kPa [b]
Permeability [c]	1e-6 m/s	5.7 e-6 m/s	5e-4 m/s

[a] These parameters were calculated for calibration of the model and were not directly input to the constitutive model.

[b] A pseudo-cohesion of 15 kPa was added to the soil elements for rockfill (equivalent to 13 kPa in the octahedral space)

[c] Defined as element property

Table 3. Ground motion properties

Earthquake	Station / Component	Component	Magnitude	Rupture Distance (km)	Vs30 (m/s)	Rupture Mechanism	Seed Motion PGA (g)	Matched Motion PGA (g) §	Matched Motion Strong Motion Duration, $D_{5\text{-}95}$ (s)	Matched Motion Arias Intensity, I_a (m/s) §
2011 Tohoku, Japan	Tajiri (MYGH06)	NS	9	63.8	593	Subduction (Interface)	0.27	0.45	77.1	6.6
2010 Maule, Chile	Cerro Santa Lucia (STL)	360	8.8	64.9	1411	Subduction (Interface)	0.24	0.46	43.8	7.7
2001 El Salvador	Acajutla Cepa (CA)	90	7.7	151.8 *	Intermediate	Subduction (Intraslab)	0.1	0.45	26.4	1.8
2011 Tohoku, Japan	Matsudo (CHB002)	NS	9	356.0 *	325 †	Subduction (Interface)	0.29	0.49	29.9	1.8
2010 Maule, Chile	Cien Agronomicas (ANTU)	NS	8.8	64.6	621	Subduction (Interface)	0.23	0.53	14.8	2.6
1985 Mexico City, Mexico	La Union (UNIO)	N00W	8	83.9*	Andesite Breccia	Subduction (Interface)	0.17	0.46	23.8	3.1
2015 Illapel, Chile	Talagante (TAL)	90	8.3	140.9	1127	Subduction (Interface)	0.07	0.47	80.4	6.2
2001 Arequipa, Peru	Moquegua (MOQ)	NS	8.4	76.7	573	Subduction (Interface)	0.22	0.44	33.8	4.1
1978 Tabas, Iran	Tabas (TAB)	T1	7.35	2.05	767	Crustal (Reverse)	0.87	0.48	17.4	2.7
1985 Nahanni, Canada	Site 1 (Site 1)	1280	6.76	9.6	605	Crustal (Reverse)	1.25	0.46	8.2	2.3
1992 Cape Mendocino, CA	Cape Mendocino (CPM)	00	7.01	6.96	568	Crustal (Reverse)	1.51	0.50	5.4	0.8
1989 Loma Prieta, CA	Los Gatos-Lex. Dam (LEX)	90	6.93	5.02	1070	Crustal (Reverse Oblique)	0.41	0.46	4.7	1.5

* Hypocentral distance
† Vs20
§ IDA 1.0

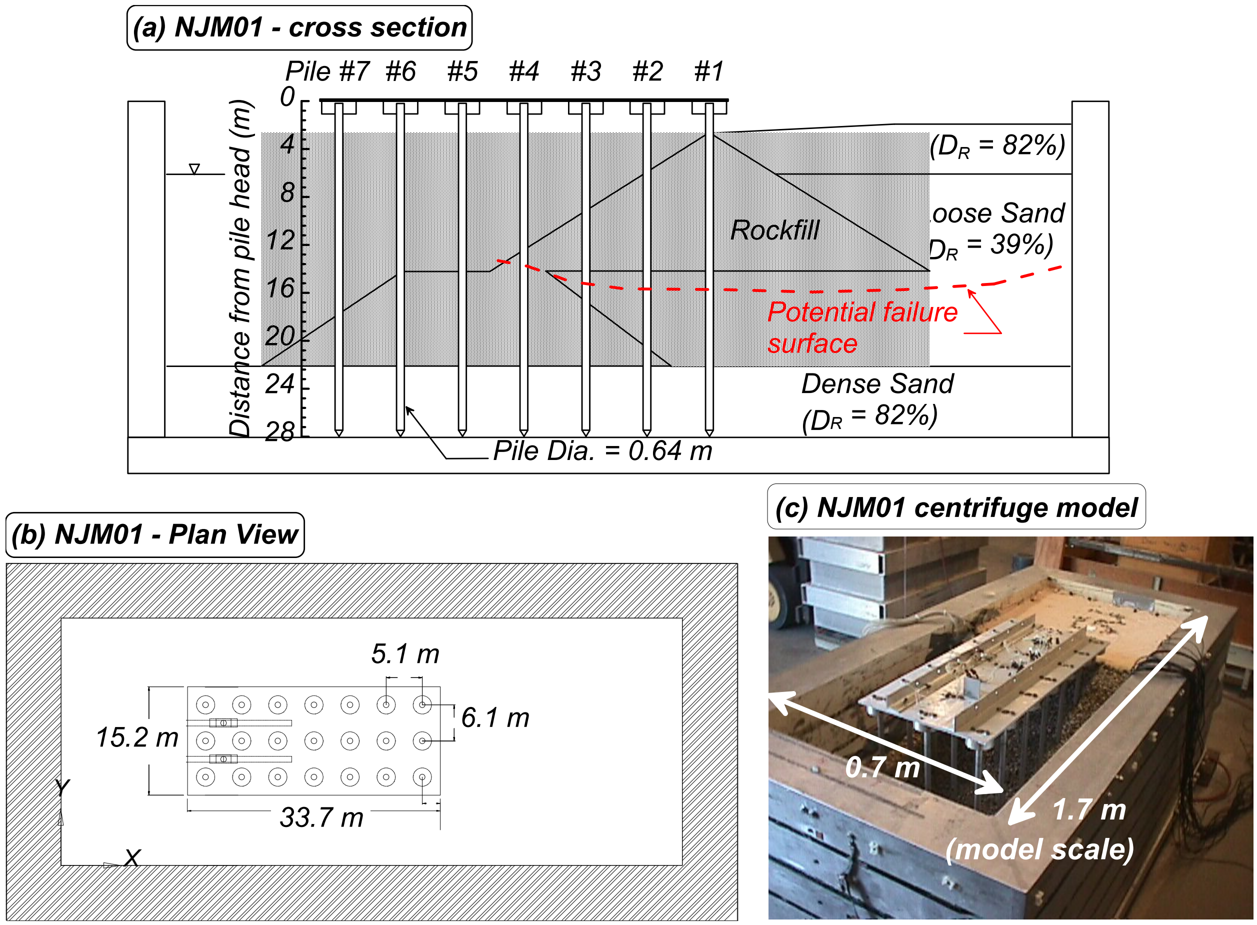

Fig. 1. Centrifuge test NJM01 layout: (a) Cross section, (b) plan view, and (c) experimental model.

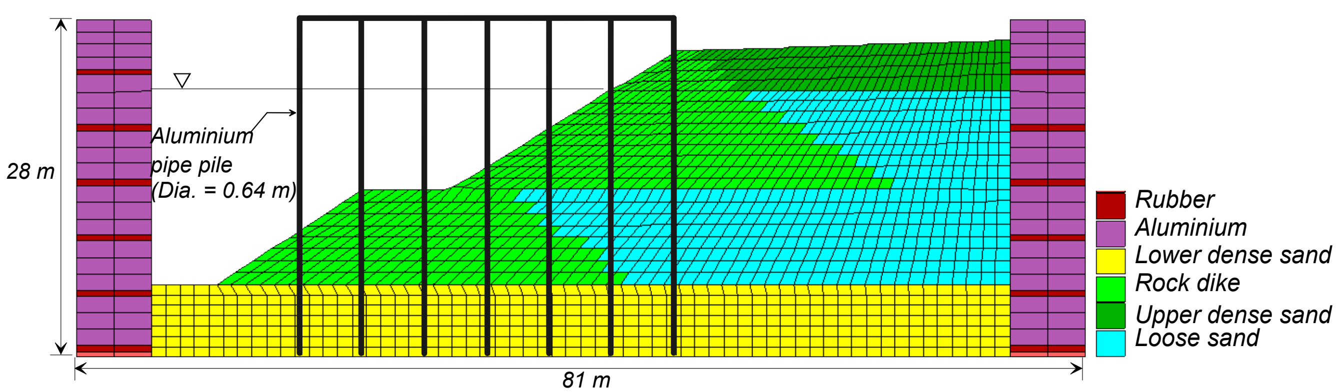

Fig. 2. The 2D *FLAC* model of centrifuge test NJM01.

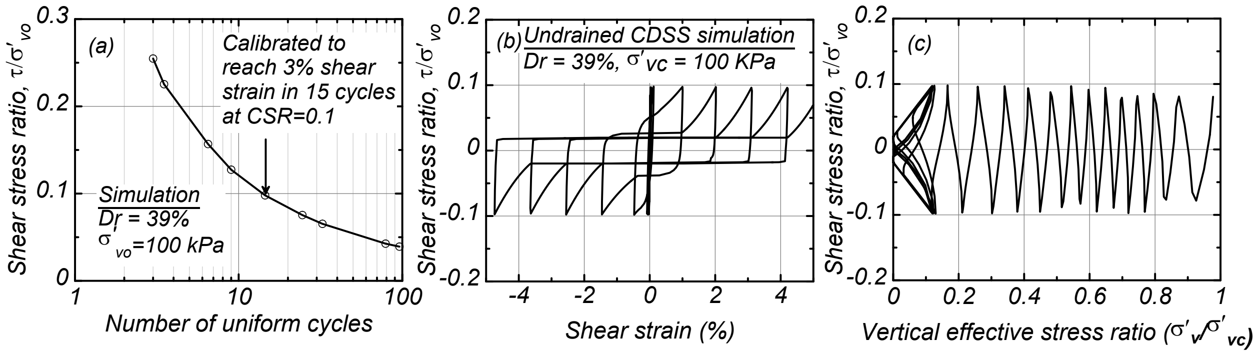

Fig. 3. Response of the soil constitutive model in undrained cyclic direct simple shear (CDSS) simulation on sand with D_R = 39%.

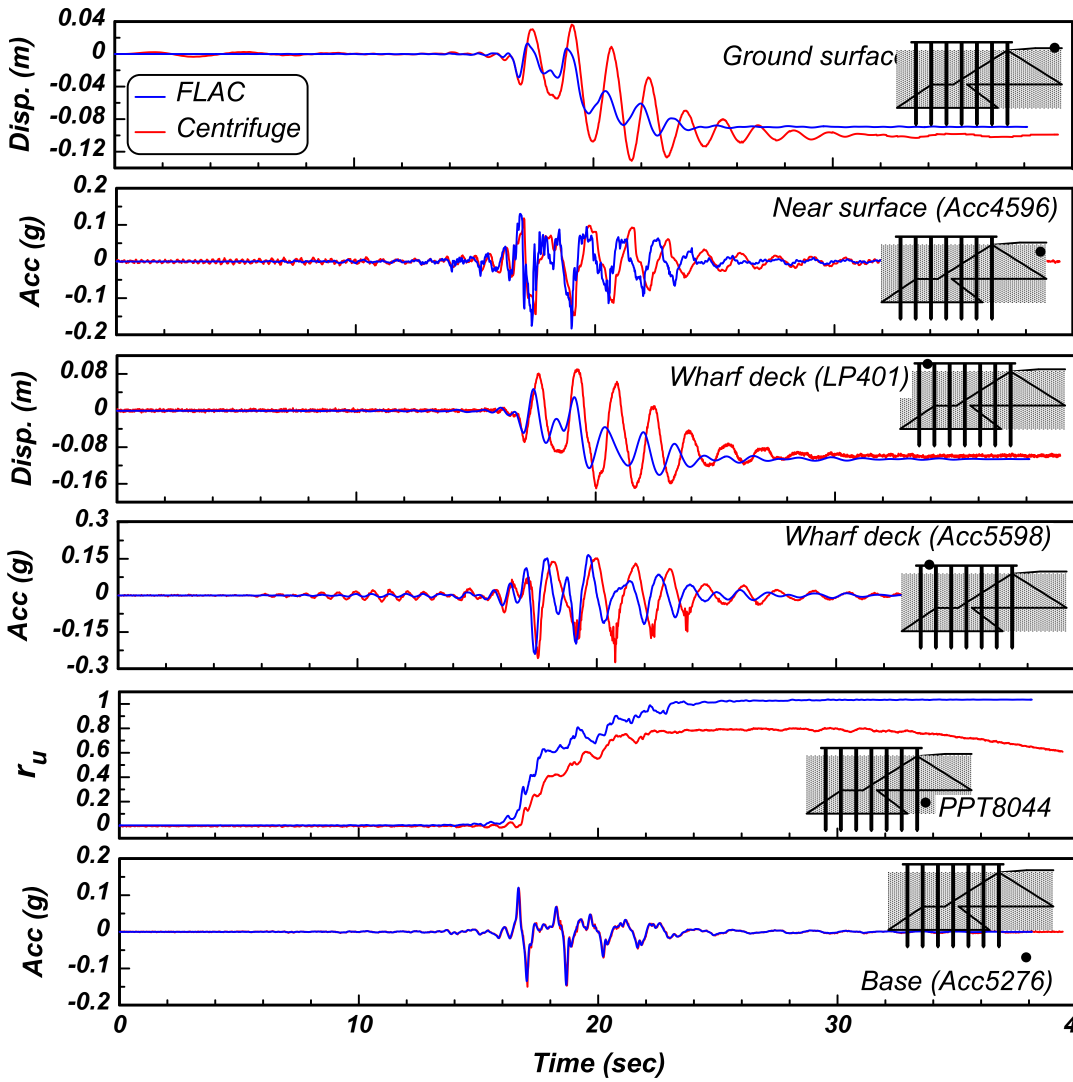

Fig. 4. Comparison of measured and computed near-field dynamic response.

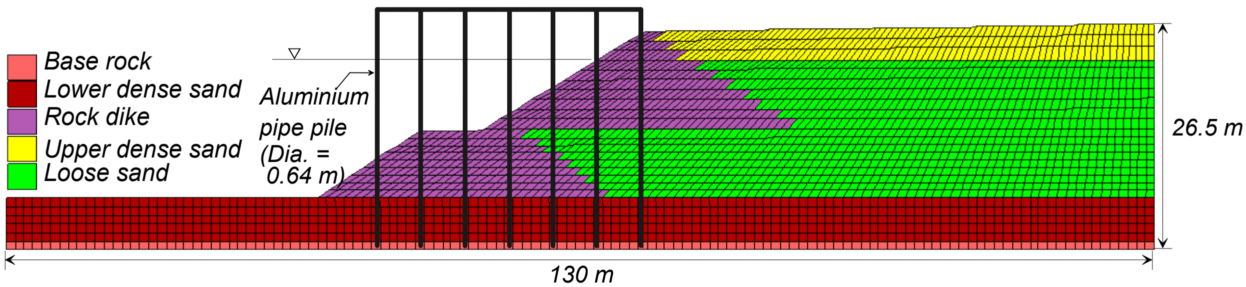

Fig. 5. Soil mesh discretization and material zones in the *FLAC* model for incremental dynamic analysis.

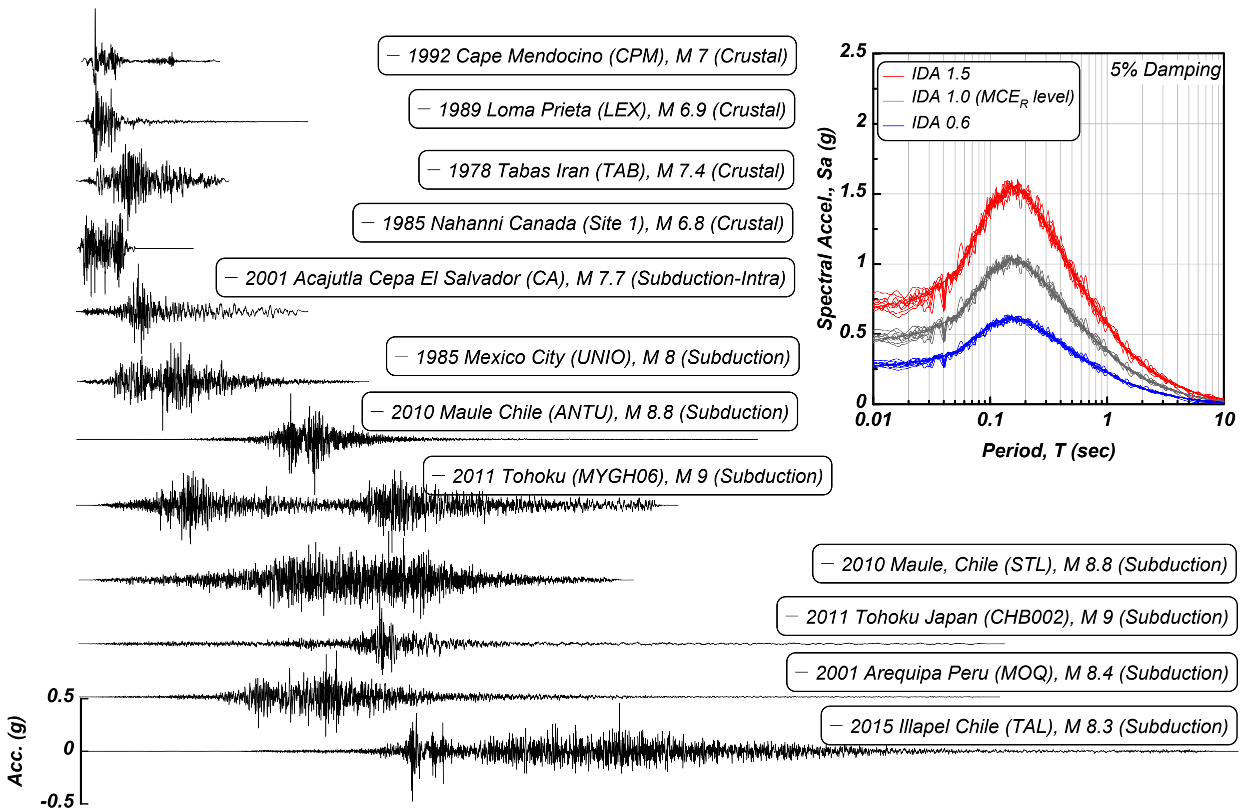

Fig. 6. Spectrally matched input motions used in the incremental dynamic analyses.

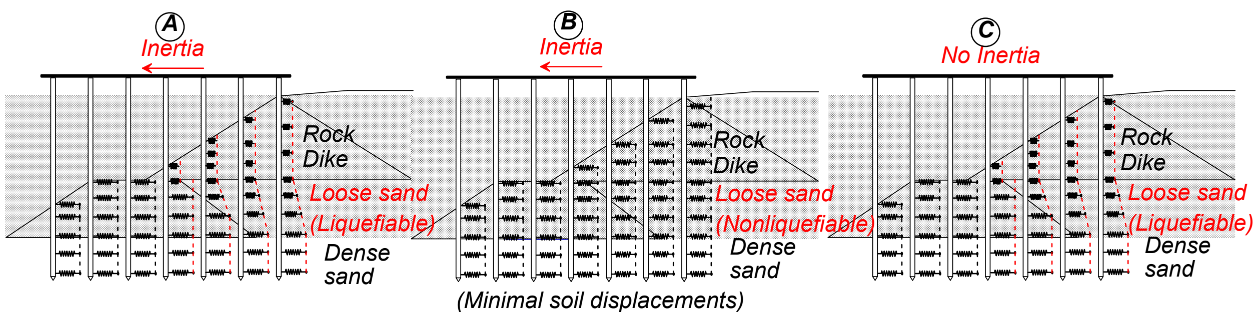

Fig. 7. Schematic of loading conditions in nonlinear dynamic analysis: (a) combined inertia and kinematics, (b) inertia only in the absence of liquefaction, and (c) kinematics only in the absence of deck mass.

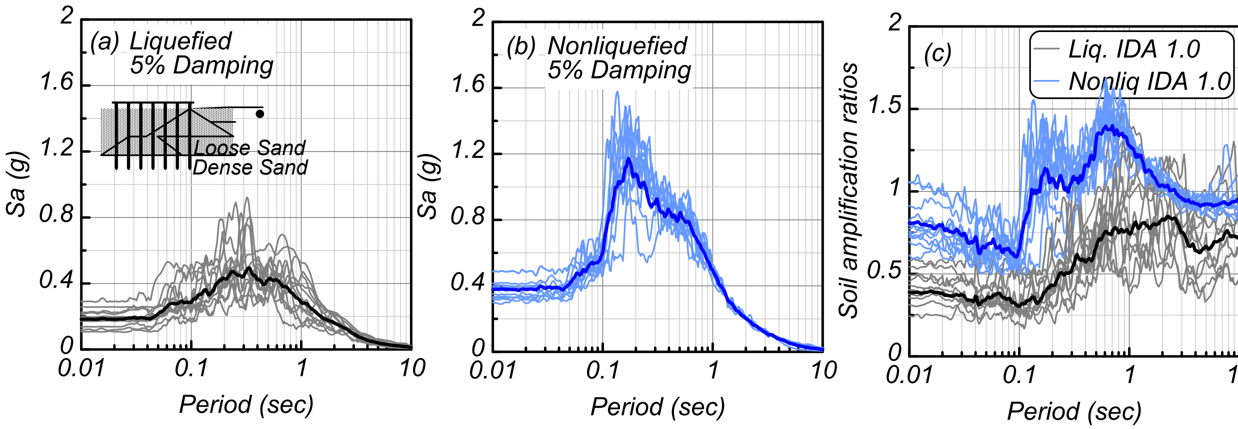

Fig. 8. Acceleration response spectra at the ground surface for (a) liquefied and (b) nonliquefied conditions; (c) soil amplification ratios with and without liquefaction. All three plots correspond to the 12 ground motions in IDA 1.0 (MCE_R level of shaking). Thick lines show geometric mean values.

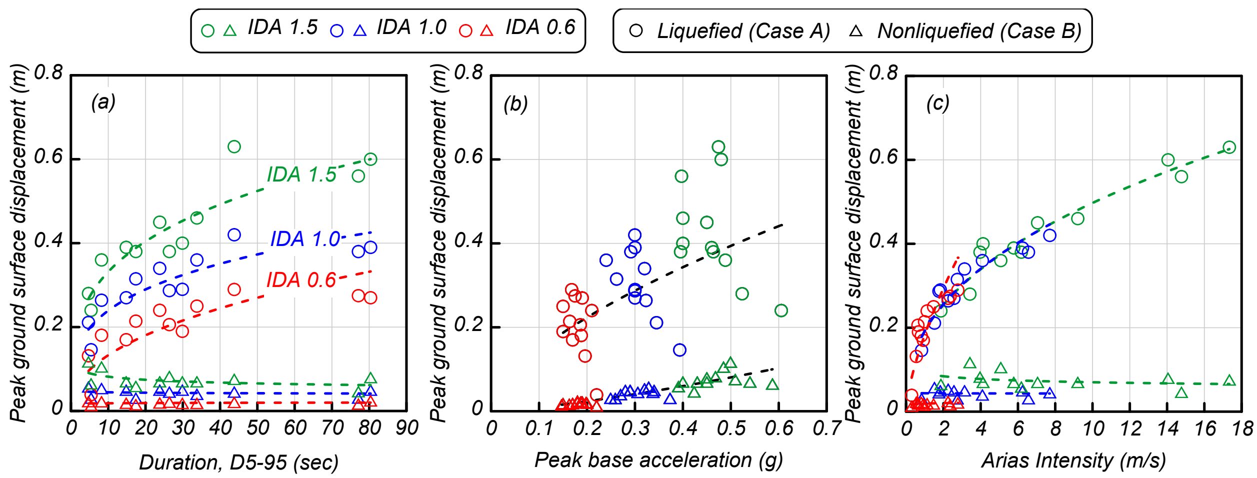

Fig. 9. Variation of peak ground surface displacement with (a) significant duration, $D_{5\text{-}95}$, (b) peak base acceleration, and (c) Arias Intensity for all motions in the incremental dynamic analyses

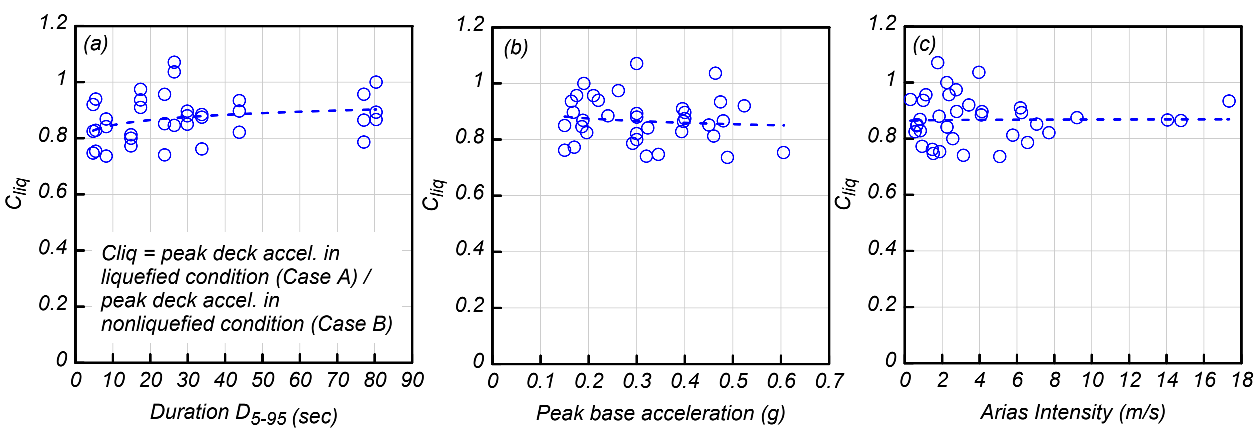

Fig. 10. Variation of the C_{liq} ratio with (a) ground motion duration ($D_{5\text{-}95}$), (b) peak base acceleration, and (c) Arias Intensity.

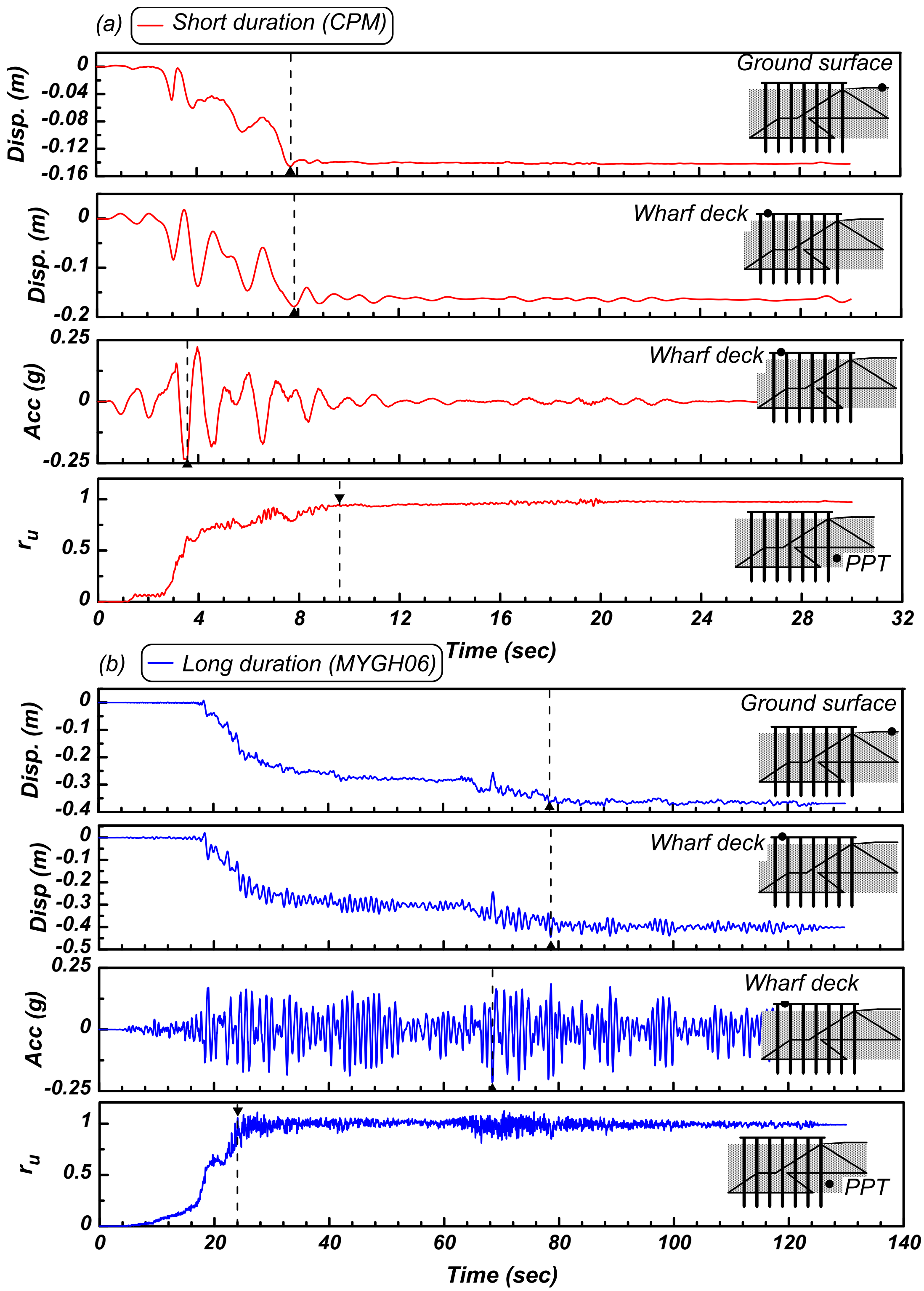

Fig. 11. Representative dynamic time histories for piles subjected to combined inertial and kinematic loads in (a) short-duration motion and (b) long-duration motion.

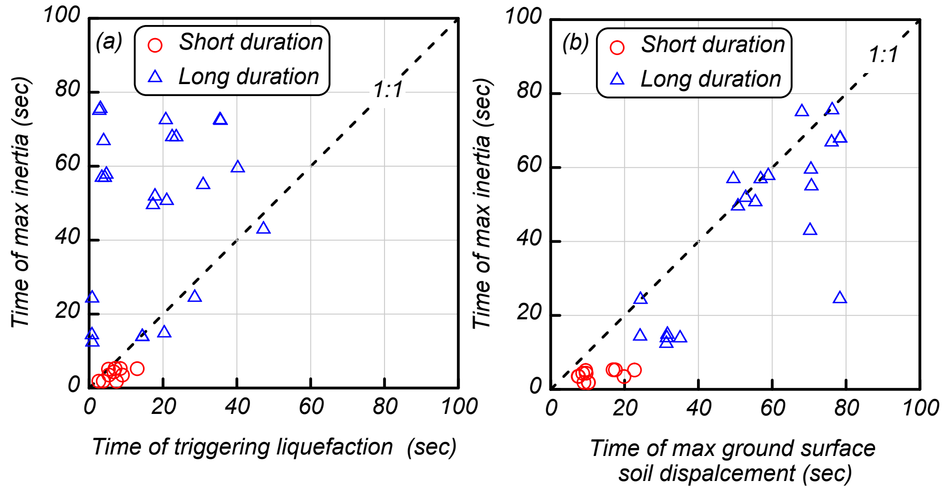

Fig. 12. Time of maximum wharf deck acceleration versus (a) time at which liquefaction is triggered, and (b) time of maximum ground surface displacement.

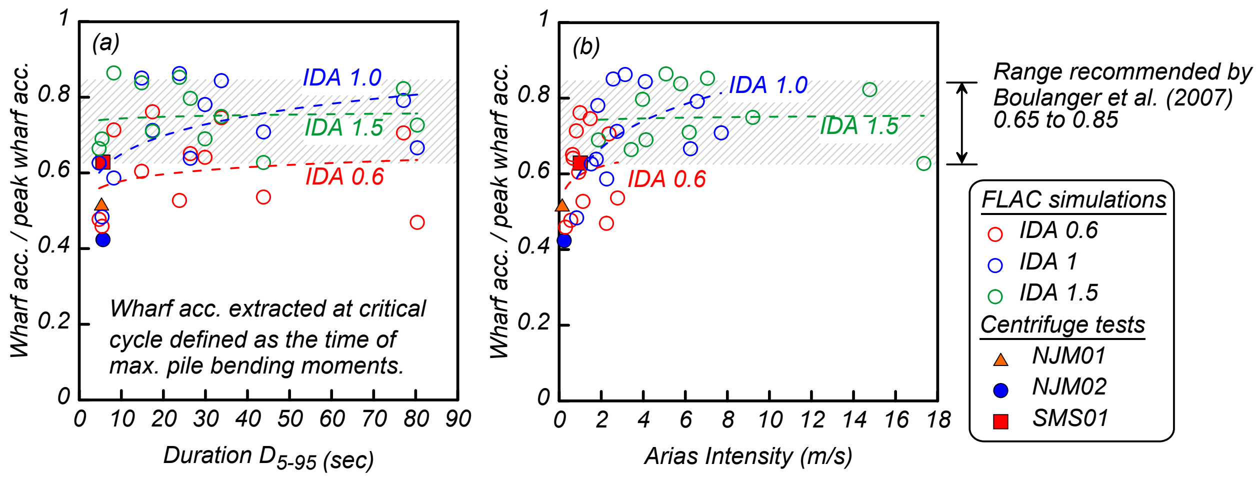

Fig. 13. Normalized wharf deck accelerations against (a) significant motion duration ($D_{5\text{-}95}$) and (b) Arias Intensity at the time of maximum pile bending moments

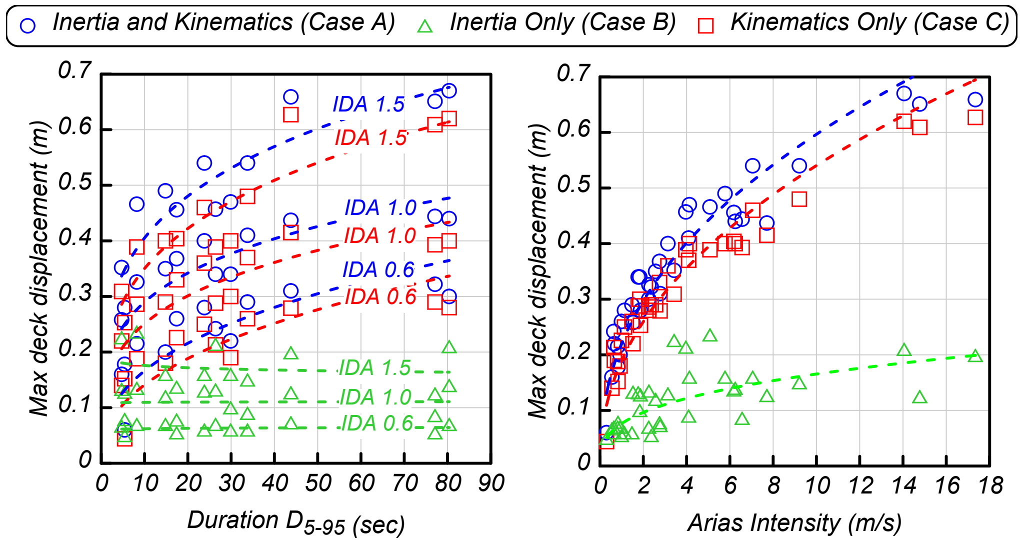

Fig. 14. Variation of maximum wharf deck displacement with (a) motion duration and (b) Arias Intensity for combined inertia and kinematics (Case A), inertia only (Case B), and kinematics only (Case C).

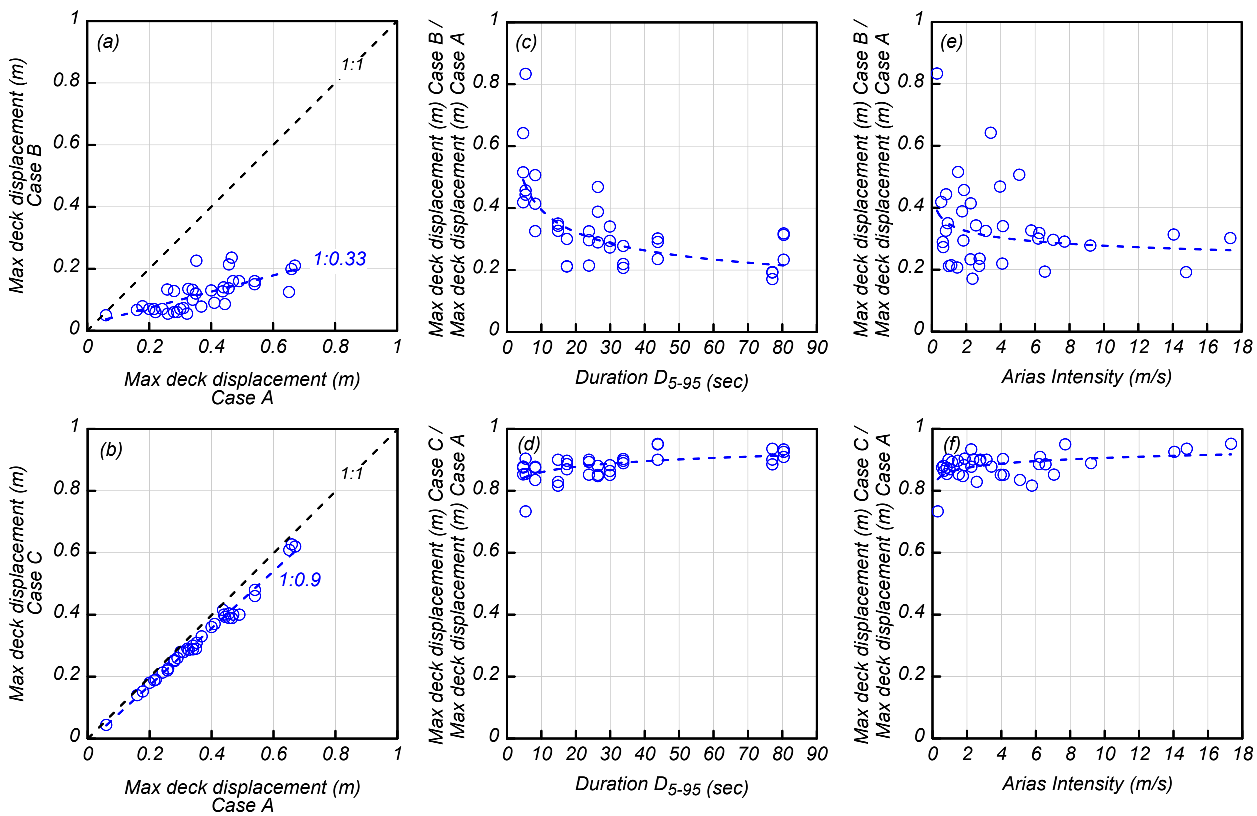

Fig. 15. Comparison of maximum wharf deck displacement in incremental dynamic analyses for combined inertia and kinematics (Case A), inertia only (Case B), and kinematics only (Case C).

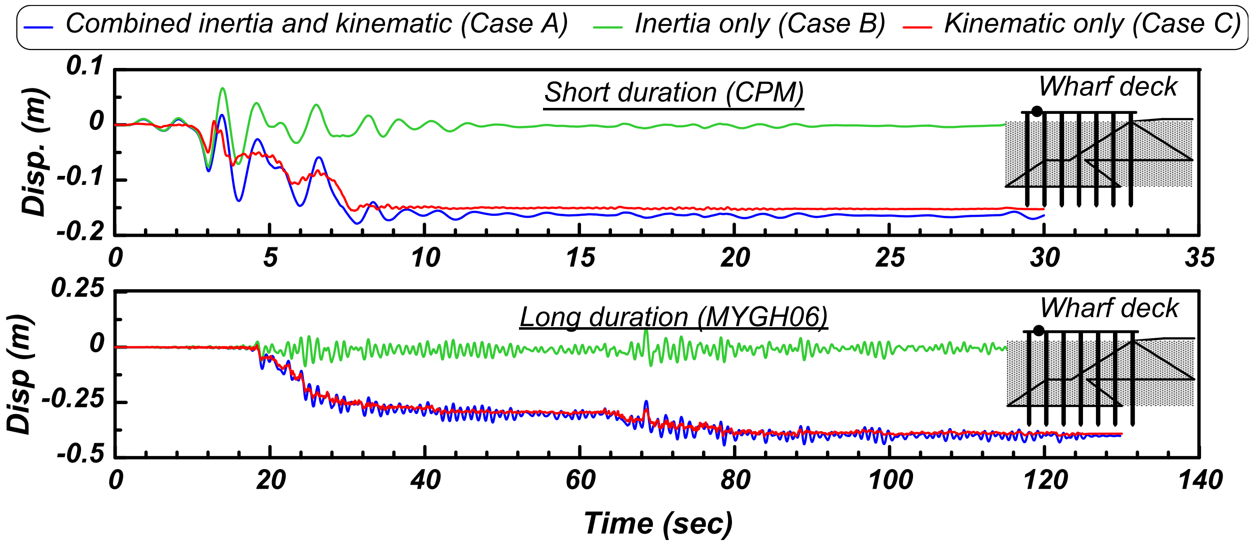

Fig. 16. Comparison of wharf deck displacements in a short- and long-duration motions for the cases of combined inertia and kinematic (Case A), inertia only (Case B), and kinematic only (Case C).